Science of the Total Environment 919 (2024) 170752

Contents lists available at ScienceDirect

Science of the Total Environment

journal homepage: www.elsevier.com/locate/scitotenv

Cu transport and complexation by the marine diatom *Phaeodactylum tricornutum*: Implications for trace metal complexation kinetics in the surface ocean

Melchor González-Dávila [a,*], Maria T. Maldonado [b], Aridane G. González [a], Jian Guo [b], David González-Santana [a], Antera Martel [c], J. Magdalena Santana-Casiano [a]

[a] Instituto de Oceanografía y Cambio Global, IOCAG, Universidad de Las Palmas de Gran Canaria, ULPGC, Spain
[b] Department of Earth, Ocean, and Atmospheric Sciences, University of British Columbia Vancouver, BC, Canada
[c] Banco Español de Algas, Instituto de Oceanografía y Cambio Global, IOCAG, Universidad de Las Palmas de Gran Canaria, ULPGC, Spain

HIGHLIGHTS

- Two Cu-binding organic ligand types were released by *P. tricornutum*
- Two putative Cu-binding sites at the cell surface of *P. tricornutum* were identified
- Only the high-affinity, Cu-binding sites exhibit reductase activity
- High-affinity Cu transporter *Pr*CTR49224 has high homology to *Homo sapiens h*CTR1, able to reduce Cu before internalization.
- The data show a link between phytoplankton metal transporters and trace metal availability/speciation.

GRAPHICAL ABSTRACT

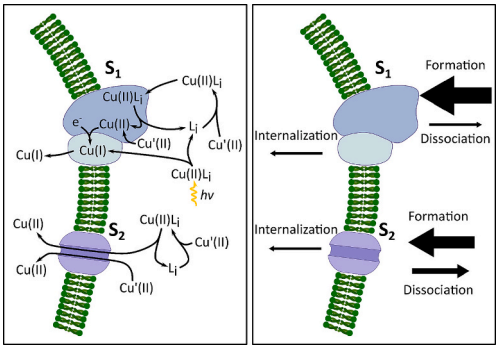

ARTICLE INFO

Editor: Julian Blasco

Keywords:
Copper
Adsorption kinetics
Cu transport
Complexation
Diatoms
Phaeodactylum tricornutum
Cu uptake

ABSTRACT

Elucidating whether dissolved Cu uptake is kinetically or thermodynamically controlled, and the effects of speciation on Cu transport by phytoplankton will allow better modeling of the fate and impact of dissolved Cu in the ocean. To address these questions, we performed Cu physiological and physicochemical experiments using the model diatom, *Phaeodactylum tricornutum*, grown in natural North Atlantic seawater (0.44 nM Cu). Using competitive ligand equilibration-cathodic stripping voltammetry (CLE-CSV), we measured two organic ligand types released by *P. tricornutum* to bind Cu (L_1 and L_2) at concentrations of ~0.35 nM L_1 and 1.3 nM L_2. We also established the presence of two putative Cu-binding sites at the cell surface of *P. tricornutum* (S_1 and S_2) with log *K* differing by ~5 orders of magnitude (i.e., 12.9 vs. 8.1) and cell surface densities by 9-fold. Only the high-affinity binding sites, S_1, exhibit reductase activity. Using voltammetric kinetic measurements and a theoretical kinetic model, we calculated the forward and dissociation rate constants of L_1 and S_1. Complementary ^{67}Cu uptake experiments identified a high- and a low-affinity Cu uptake system in *P. tricornutum*, with half-saturation

* Corresponding author.
E-mail addresses: melchor.gonzalez@ulpgc.es (M. González-Dávila), mmaldonado@eoas.ubc.ca (M.T. Maldonado), aridane.gonzalez@ulpgc.es (A.G. González), jguo@eoas.ubc.ca (J. Guo), David.gonzalez@fpct.ulpgc.es (D. González-Santana), antera.martel@ulpgc.es (A. Martel), Magdalena.santana@ulpgc.es (J.M. Santana-Casiano).

https://doi.org/10.1016/j.scitotenv.2024.170752
Received 26 October 2023; Received in revised form 30 January 2024; Accepted 4 February 2024
Available online 9 February 2024

constant (K_m) of 154 nM and 2.63 μM dissolved Cu, respectively. In the *P. tricornutum* genome, we identified a putative high-affinity Cu transporter (*Pt*CTR49224) and a putative ZIP-like, low-affinity Cu transporter (*Pt*ZIP49400). *Pt*CTR49224 has high homology to *Homo sapiens h*CTR1, which depending on the accessibility to extracellular reducing agents, the *h*CTR1 itself is involved in the reduction of Cu^{2+} to Cu^{+} before internalization. We combined these physiological and physicochemical data to calculate the rate constants for the internalization of Cu, and established that while the high-affinity Cu uptake system (S_1) is borderline between a kinetically or thermodynamically controlled system, the low-affinity Cu transporters, S_2, is thermodynamically-controlled. We revised the inverse relationship between the concentrations of inorganic complexes of essential metals (i.e., Ni, Fe, Co, Zn, Cd, Mn and Cu) in the mixed layer and the formation rate constant of metal transporters in phytoplankton, highlighting the link between the chemical properties of phytoplankton metal transporters and the availability and speciation of trace metals in the surface ocean.

1. Introduction

Copper is an essential redox-active metal for phytoplankton, acting as a cofactor of electron-transfer proteins in respiration (i.e., cytochrome *c*-oxidase, (Merchant et al., 2006), in oxidative stress (i.e., superoxide dismutase, Chadd et al., 1996), in photosynthesis (i.e., plastocyanin; Nosenko et al., 2006; Peers and Price, 2006) and/or organic nitrogen assimilation (i.e., amine oxidases, Palenik et al., 1989). Copper is also involved in the high-affinity iron (Fe) transport systems in yeast, green unicellular algae and coastal and oceanic diatoms (Askwith et al., 1994; La Fontaine et al., 2002; Maldonado et al., 2006). However, at high levels, Cu can become toxic, producing hydroxyl radicals (Halliwell and Gutteridge, 1990) that cause oxidative damage to lipids, proteins and DNA (Herzi et al., 2013; Juneau et al., 2002; Long et al., 2019) and changes the content of amino acids in the cell (Santiago-Díaz et al., 2023).

The concentrations of dissolved Cu in the open ocean range from 0.5 to 6 nM and are not considered toxic (Coale and Bruland, 1990; Sunda et al., 1990; Ruacho et al., 2022). However, high levels of dissolved Cu are observed in some coastal regions (i.e., up to 150 nM) and are associated with anthropogenic Cu inputs, such as municipal effluents (Johannessen et al., 2015), mining (Chretien, 1997), antifouling agent-coated ships (Carić et al., 2021), and/or urban stormwater (Barałkiewicz et al., 2014). These high Cu concentrations may be toxic to the biota in coastal waters (Moffett et al., 1997).

However, the vast majority of dissolved Cu (>99 % of dCu) in the ocean is complexed by a heterogeneous pool of natural organic ligands, which form stable, less bioavailable organic complexes that buffer against Cu toxicity (Barber and Ryther, 1969; van den Berg et al., 1987; Buck et al., 2007, 2010). Cu-binding ligands are often produced by phytoplankton during toxic conditions (Moffett and Brand, 1996; Dupont et al., 2004) and Cu limitation (Kim et al., 2008; Walsh et al., 2015) or are of terrestrial origin, such as humic substances in river water (Laglera et al., 2007; Whitby and van den Berg, 2015; Ruacho et al., 2022) and biological macromolecules in municipal wastewater (Sarathy and Allen, 2005).

Given the essential role of Cu in phytoplankton physiology and its possible toxicity, elucidating cellular Cu requirements, the potential components of Cu transport and homeostasis in phytoplankton are of interest. However, this has been difficult due to the lack of a commercially available, long-lived Cu radiotracer. In the last 20 years, several studies have been published on the Cu quotas of marine phytoplankton grown under various environmental conditions and their Cu uptake systems (i.e., Annett et al., 2008; Guo et al., 2010; Guo, 2012 and references within). From these studies, we have learned that their Cu requirements are modulated by Cu availability and their Fe status. We have also revealed that diatoms, for example, have low- and high-affinity Cu transport systems with distinct uptake kinetics (Guo et al., 2010). Furthermore, molecular studies suggest that the low-affinity Cu transporters are probably non-specific divalent transporters, such as NRAMPs (i.e., the Natural Resistance-Associated Macrophage Protein) or ZIP (i.e., Zrt/IRT-like proteins) (Guo et al., 2015). Diatoms and indigenous phytoplankton in the NE subarctic Pacific can also access Cu bound within organic Cu complexes by cell surface cupric reductases (Semeniuk et al., 2009, 2015), indicating that dissolved Cu species may control Cu uptake, and not just free or inorganic Cu (Guo et al., 2010).

These findings were somewhat surprising because many previous studies have documented the production and release of strong organic ligands for Cu by a variety of phytoplankton to decrease Cu toxicity, especially in coastal environments. The production of strong organic ligands for Cu can affect Cu bioavailability and physicochemical processes related to its sorption onto and precipitation of particles.

Given that phytoplankton can release strong organic complexes for Cu to lower toxicity, as well as take up Cu via low and high-affinity transport systems, in this study we aimed to characterize the complexing properties of the strong organic ligands for Cu release in solution, as well as those at the cell membrane that might be involved in Cu acquisition. We use a combination of voltammetric measurements and physiological studies. We chose the marine diatom *P. tricornutum* as a model because of its ability to release organic complexes for Cu, and its sequenced genome (Allen et al., 2008). We first studied *P. tricornutum* uptake kinetics of Cu transport, from 1 nM to 2000 nM, using the radiotracer ^{64}Cu. Since high Cu adsorption on the cell surface of microbes is common (Beveridge and Murray, 1980; de Lurdes et al., 1987; González et al., 2010; Gonzalez-Davila et al., 1995; González-Dávila et al., 2000; Fein et al., 1997), we also investigated *P. tricornutum* Cu adsorption capacity at low nanomolar levels. These studies allowed us to explore the possible competition between the Cu-binding ligands in solutions and those onto the cell surfaces. In all the experiments, we used natural seawater from the vicinity of the Canary Islands, which was, when appropriate, enriched with nutrients, sterilized and/or UV-irradiated to remove the natural organic compounds in seawater. Ultimately, we aim to elucidate the competition between strong Cu-binding ligands in solutions and those at the cell surface, and its effects on Cu acquisition by phytoplankton in the open ocean.

2. Material and methods

2.1. Chemicals for cultures

2.1.1. Nutrients

A concentrated stock solution of 0.3 M sodium nitrate (Sigma), 0.01 M potassium hydrogen phosphate (Sigma), and 0.1 M sodium silicate (Sigma) was prepared in 250 mL acid-cleaned bottles. Contaminating metals were removed by using 100 μM MnO_2 (Van Den Berg, 1982), equilibrated overnight and filtered through acid-cleaned 0.2 μm pore-size filters (Whatman, 25 mm GD/X Sterile, CA filter media with polypropylene housing). The final concentrations of nitrate, phosphate and silicic acid in the culture media were $3 \cdot 10^{-4}$, $1 \cdot 10^{-5}$ and $1 \cdot 10^{-4}$ M, respectively. While not in use, the stocks were kept in the dark and the fridge.

2.1.2. Vitamins

The final concentrations of vitamins in our media were identical to those of the f/2 media (Guillard and Ryther, 1962), such that the concentrations of cyanocobalamin (vitamin B_{12}), Biotin (vitamin H) and

Thiamine HCL (vitamin B_1) were 3.69×10^{-10}, 2.05×10^{-9} and 2.96×10^{-7} M, respectively.

2.1.3. Cyclam (Cy)

Cyclam (Cy) was added to induce low Cu stress in the cultures. Cyclam (1,4,8,11-tetraazacyclotetradecane) has a high conditional stability constant for Cu(II) binding (log $K_0 = 15.3$, Semeniuk et al., 2015) and can maintain [Cu] at subfemtomolar levels. The 12.5 mM primary Cy stock was prepared by dissolving 0.12 g of Cy (1,4,8,11-tetraazacyclotetradecane, MW 200.32 g mol^{-1}; Sigma-Aldrich) in 4 mL of methanol (Honeywell Chromasolv) and brought up to 50 mL using sterilized Ultra Pure Water (UPW; 18.2 MΩ cm at 25 °C). A secondary stock of $2 \cdot 10^{-4}$ M was produced by diluting the primary stock with UPW. The final concentration of Cyclam was 200 nM in the culture medium.

2.2. Culture characterization

An axenic culture of the diatom *P. tricornutum* (UTEX 646, isolated in 1951 by M.R. Droop in Segelskär, Finland) was obtained from the Spanish Bank of Algae in Gran Canaria (Spain), and maintained in f/2 media (Guillard, 1975), at constant temperature (24 °C) and light intensity (110–120 μE m^{-2} s^{-1}) in a culture chamber (Friocell 111). Sterile, trace metal clean techniques (e.g., Leal et al., 2016) were used during all experiments and manipulations in this study.

2.3. The growth media for the adaptation of the P. tricornutum cells

The natural seawater used for culture media was collected in February 2018 from the European Time-Series Station in the Canary Islands (ESTOC; 29° 10′ N 15° 30′ W) within the oligotrophic North Atlantic subtropical gyre. The seawater was collected at 20 m depth using a trace metal clean Teflon pump (PFD2 316F, AstiPure®) and filtered by 0.2 μm dual pore-size trace metal clean filters (Acropack™). The seawater was analyzed for trace metal concentration (Table S1) within 12 months after collection on a SF-HR-ICP-MS Element XR instrument (Thermo Fisher, Bremen, Germany) coupled with an online seaFAST system (Elemental ScientificTM), at Pôle Spectrométrie Océan (IFREMER, France) (González-Santana et al., 2020).

Two different media were prepared for the *P. tricornutum* cell cultures. The natural ESTOC media were sterilized by heating for 12 min (3 min in 4 times to avoid overheating) in a 700 watts microwave. This sterilized natural ESTOC seawater was enriched with filtered-sterilized nutrients and vitamins, and referred to as SW(nut + VIT). The control media had no Cyclam addition, and was called CO_{MEDIUM} (i.e., SW(nut + VIT)), while the low Cu stress media had 200 nM Cyclam, and was named Cy_{MEDIUM} (i.e., SW(nut + VIT + Cy)).

Semi-continuous batch cultures (Paasche, 1973, 1977; Brand, 1985) were used to adapt *P. tricornutum* to the different growth media. In essence, once the cells in the media were approaching mid to late exponential growth, they were transferred to new media (CO_{MEDIUM} or Cy_{MEDIUM}) using a proportion between 20:80 and 10:90 (medium with cells: medium without cells) depending on their growth rate. In the triplicate cultures, the cells were counted daily using a light microscope (Olympus BH2) a hemacytometer, and a Flow cytometer (BECKMAN COULTER® Cell lab Quant™ SC). The exponential, absolute growth rates were calculated in days using ln (μ, d^{-1}). These absolute growth rates were converted to doublings per day (*k*, dd^{-1}) by dividing μ by the ln of 2. The acclimation was assumed to be achieved when the growth rates among successive transfers did not differ by >15 % (Wood et al., 2005), normally taking four to five transfers. The average growth rates were 0.94 ± 0.44 d^{-1} and 0.97 ± 0.30 d^{-1} in the CO_{MEDIUM} and the Cy_{MEDIUM}, respectively (Table S2).

Cell surface measurements were performed, assuming that the fusiform morphology of *P. tricornutum* resembles an ellipse (Bartual et al., 2008). The size measurements were performed on images taken in a Nikon Eclipse 90i automated optical microscope, equipped with a NIS-Elements AR image treatment program. The area of the ellipse was calculated considering five reference points on each cell. The surface areas (μm^2) for the different experimental conditions are included in Table S2.

2.4. Measurement of Cu uptake kinetics of the P. tricornutum

For the Cu uptake kinetic experiments, acclimated cultures in mid-exponential phase were transferred from the 28 mL tubes to 2 L fresh CO_{MEDIUM} Polycarbonate. The growth rates of the diatoms in these bottles were monitored daily. Cell density and size (μm) were also determined for live samples using a Coulter Z2 Particle Count and Size Analyzer. Cell surface area (μm^2) and volume (fL = 10^{-15} L) were determined.

Fourteen Cu concentrations were used in the Cu uptake kinetic experiments, including 2, 30, 60, 80, 100, 120, 180, 240, 300, 500, 700, 1000, 1500, and 2000 nM total Cu (Fig. 1). The non-radioactive Cu and a spike of the carrier-free tracer ^{64}Cu (0.56 MBq L^{-1}) were buffered with 100 μM EDTA in 100 mL of sterilized ESTOC SW with only nutrients SW (nut) to achieve the targeted total Cu concentrations. Given that EDTA is often used as a ligand in phytoplankton culture media and was used for Cu uptake experiments in diatom *T. pseudonana* and *T. oceanica* (Guo et al., 2010), EDTA was chosen for this experiment. The gamma-emitting radionuclide ^{64}Cu ($t_{1/2}$ = 12.7 h) was provided by Dr. Paul Schaffer's team at the Canada's particle accelerator centre TRIUMF (https://www.triumf.ca/).

After the Cu and EDTA additions, the media were allowed to equilibrate chemically for 16 h before use. The next day, trace metal clean techniques were used to filter 5 L cultures onto trace metal clean 2 μm polycarbonate (Poretics, 24 h acid-soaked) filters (47 mm) by gentle vacuum (<100 mmHg) and washed with 10 mL SW(nut). Filtered cells were immediately resuspended in 30 mL of SW(nut) and then aliquoted to 14 bottles with media spiked with ^{64}Cu and different non-radioactive Cu concentrations. The cells were incubated at room temperature and exposed to 150 μmol·quanta·m^{-2}·s^{-1}. The initial sampling time was 20 min after resuspension, followed by 30-min and 1-h sampling intervals. Fifty mL aliquots of culture were removed during the initial sampling, and 25 mL aliquots of culture were removed during the second and third

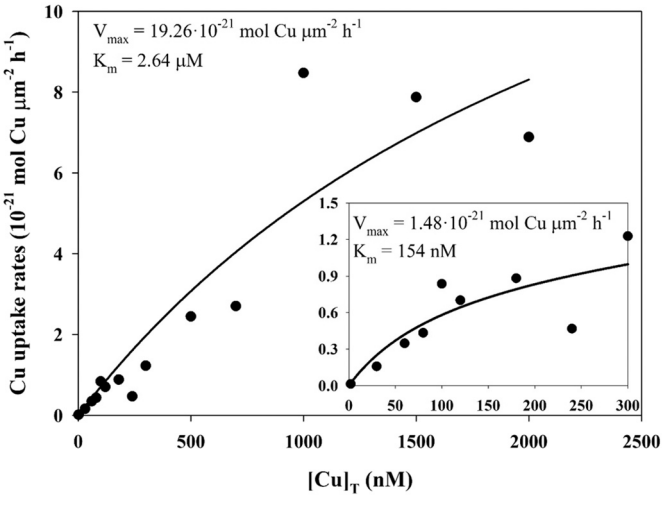

Fig. 1. Michaelis–Menten kinetics of Cu uptake as a function of total Cu concentrations in *P. tricornutum*. The data points are the rates of Cu uptake (10^{-21} mol Cu·μm^{-2}·h^{-1}) and were determined as described in the Material and methods section. The curves are the line of best fit for the single rectangular hyperbola eq. ($V = V_{max}$ $[Cu]_{total}$ / ($[Cu]_{total} + K_m$)), where V is the total Cu uptake rate (10^{-21} mol Cu·μm^{-2}·h^{-1}), V_{max} is the maximum Cu uptake rates, $[Cu]_{total}$ is the total Cu concentration (nM), and K_m is the half-saturation constants of the Cu uptake system.

sampling. Cells were vacuum filtered onto a 2 μm, 25 mm polycarbonate membrane. The filtered cells were soaked for 5 min with 5 mL of 1 mM diethylenetriaminepentaacetic acid (DTPA) solution (dissolved in sterile SOW, pH_{NBS} adjusted to 8.14; (Croot et al., 1999) to bind the extracellular adsorbed ^{64}Cu, then washed with 5 mL SW(nut). The radioactive filters were placed in scintillation vials; radioactivity was determined using a PerkinElmer 1480 WIZARD 3″ Gamma Counter. Duplicate initials (1 mL) of the uptake medium were also taken to determine the specific activity of ^{64}Cu in the uptake media (MBq $^{64}Cu/Cu'$ concentration added). At the end of each ^{64}Cu uptake experiment, a sample was fixed with Lugol's solution to determine cell density using the Coulter Z2 Particle Count after the ^{64}Cu had decayed.

Using the statistical program SigmaPlot 13.0 (Systat Software Inc.), the Cu uptake rates (10^{-27} mol $Cu'\cdot\mu m^{-2}\cdot h^{-1}$) for each Cu concentration were determined by linear regressions of the accumulation of Cu as a function of time, and were then used to calculate the V_{max} and K_m of Cu transport, using the Michaelis–Menten eq. ($V = V_{max}\,[Cu]/([Cu] + K_m)$, where V is the total Cu uptake rate, V_{max} is the maximum uptake rates of the Cu uptake systems, [Cu] is the total dissolved Cu concentration. As the data were clearly biphasic, we calculated kinetics parameters for 0–300 nM Cu and for 0–20,000 nM Cu, the high- and low-affinity transport system, respectively. The standard errors associated with the V_{max} and K_m parameters are those from the best-fit values (Table 1, Fig. 1). The K_m were also calculated as a function of dissolved inorganic Cu (pM Cu′), using the equation $[Cu'] = [Cu_T]/(1 + K_{EDTACu'}[EDTA] + 0.01\,K_{Cu'L_1}[L_1] + 0.01K_{Cu'L_2}[L_2])$, where K is the conditional stability constant of the ligands released by *P. tricornutum* in the culture media (see below). The K_m for Fe as [Fe′] for *T. weissflogii* was reported in Table 2 in Hudson and Morel (1990). We converted this Fe′ concentration to total Fe concentration using their Fig. 6, where they report [Fe'] as a function of total Fe in their uptake experiments (i.e., $\log [Fe'] = (0.8602 * \log [Fe]_{total}) - 3.181$).

2.5. Chemicals for Cu ligand complexation and cellular Cu adsorption

The Cu stock solutions were prepared using Cu atomic absorption spectrometry standard solution (1000 mg L^{-1}, Fluka in 2 % HNO_3). Diluted Cu stock solutions ranging between 100 and 3000 nM were prepared in 12 mM HCl (ultrapure, Merck).

An aqueous stock solution containing 0.01 M salicylaldoxime (SA, Sigma-Aldrich) in 0.1 M HCl (ultrapure, Merck) was used to determine the Cu concentration in seawater. A pH buffer containing 1 M 4-(2-Hydroxyethyl) piperazine-1-propanesulfonic acid (EPPS, Sigma-Aldrich) in 1 M NH_4OH (ultrapure, Fluka) was prepared at pH_F 8.2 similar to (Campos and van den Berg, 1994). Contaminating metals were removed from the pH buffer using 100 μM MnO_2 (Van Den Berg, 1982). All solutions were prepared with UPW.

Table 1
Kinetic parameters of the Cu-transport system in *P. tricornutum*. The K_m and V_{max} values (± standard error of best-fit value) were calculated for the Cu-uptake rates measured at Cu concentrations ranging from 2 nM to 2000 nM. The uptake parameters were calculated using the Michaelis–Menten eq. ($V = V_{max}\,[Cu]_{total}$ / ($[Cu]_{total} + K_m$)), where V is the total Cu uptake rate (10^{-21} mol $Cu\cdot\mu m^{-2}\cdot h^{-1}$), V_{max} is the maximum Cu uptake rates, $[Cu]_T$ is the total Cu concentration (nM), and K_m (nM total Cu) is the half-saturation constants of the Cu uptake system. The K_m, as dissolved inorganic Cu (pM Cu′), was calculated by equation $[Cu'] = [Cu]total / (1 + K'_{EDTACu'}[EDTA] + 0.01\,K'_{L1Cu'}[L_1] + 0.01\,K'_{L2Cu'}[L_2])$, where K' is the conditional stability constant of the ligand in the culture media. R^2 is the regression coefficient of the Michaelis–Menten equation fit to the data.

$[Cu]_{total}$	Kinetic parameters	Value	R^2
0–2000 nM	V_{max} (10^{-21} mol $Cu\cdot\mu m^{-2}\cdot h^{-1}$)	19.3 ± 10.6	0.86
Low-affinity	K_m (nM total Cu)	2636 ± 2156	
	K_m (pM Cu′)	1.37 ± 1.12	
0–300 nM	V_{max} (10^{-21} mol $Cu\cdot\mu m^{-2}\cdot h^{-1}$)	1.48 ± 0.60	0.77
High-affinity	K_m (nM total Cu)	154 ± 130	
	K_m (pM Cu′)	0.08 ± 0.07	

2.6. The conditioning media and study solutions for the experiments on Cu ligand complexation and cellular Cu adsorption

The natural, filtered ESTOC seawater was UV irradiated (Ultra-Violet photo-oxidation unit 7900-74 Ace Glass) for 4 h to remove any natural organic ligand, which was confirmed by voltammetric determinations (see below). Before the Cu complexation and sorption experiments, the acclimated cells (in CO_{MEDIUM} or Cy_{MEDIUM}) were transferred to the so-called *conditioning media*, which consisted of UV-irradiated ESTOC seawater, without vitamins, but with additions of nutrients and Cyclam.

To transfer the acclimated cells from the growth media to the *conditioning media* and to avoid cell breaking, 1000 mL of acclimated cell culture were gravity filtered (1.2 μm trace metal acid clean pore-size nitrocellulose, Sarthorius™). Filters with the cells were rinsed five times with 20 mL of the corresponding 'conditioning media' to remove vitamin excess. The transfer was concluded by introducing the filter with the cells into ~500 mL of *conditioning media*. The cells in the *conditioning media* were then counted to ensure proper cell concentrations and checked to confirm that they remained morphologically intact. The *conditioning media* with the cells were then placed in the culture chamber for a maximum of 3 h.

After this period, the 500 mL of the *conditioning media* with the cells was gravity filtered onto a 1.2 μm pore-size nitrocellulose filter (Sarthorius™). The cells were rinsed five times each with 20 mL of UV-irradiated and sterilized seawater and were then re-suspended in ~200 mL UV-irradiated and sterilized seawater, free of Cyclam (named here *study solution*), ensuring final cell concentrations of $25–80 \cdot 10^3$ cell mL^{-1} (Tables 2 and 3). The cells in the *study solution* were counted and checked for intactness once more and were then used for the Cu ligand complexation and cellular Cu adsorption studies.

2.7. Voltammetric determination of Cu speciation

A voltammetric system (Epsilon Basi, Inc.) connected to a hanging mercury drop electrode (CGME, Basi, Inc.) was used for the Cu speciation analysis. The reference electrode was Ag/AgCl with a salt bridge filled with 3 M KCl, with a platinum auxiliary electrode. A magnetic stirrer mixed the solutions during the deposition step. Oxygen was removed by purging with 0.2 μm filtered high-purity nitrogen gas (99.9995 %, Carburos Metálicos). The first two drops of the mercury drop electrode were always discarded, and the third mercury drop was used. Voltammetric cells (PTFE) used for the copper determination were cleaned with 0.1 M HCl and rinsed with MQ water. The Teflon vials were always conditioned overnight with trace metal-clean seawater before the experiments.

2.8. Excreted Cu-binding ligands studies

The cells in the *study solution* were allowed to excrete Cu-binding ligands for 3 min to 24 h, depending on the culture and date (see Table 2). Approximately, ~200 mL of each *study solution* was filtered onto a 0.45 μm pore-size filter (acid-clean nitrocellulose, Sarthoriu™). In this *filtrate solution,* we determined the concentration of total dissolved Cu (Cu_T) and ligands, as well as the complexing constants.

Total dissolved Cu concentration (Cu_T) in the *filtrate solution* was determined by Differential Pulse Cathodic Stripping Voltammetry (DPCSV) using four standard additions and SA as a competitive ligand. Ten mL of the filtered *study solution* were UV-irradiated for 4 h (Campos and van den Berg, 1994), followed by additions of SA (final concentration of 20 μM) and 100 μL of 1 M EPPS buffer (0.01 M final concentration) to adjust the pH_F to 8.2. The DPCSV conditions were: Deposition Potential at −50 mV for 60 s, Quiet Time for 10 s, Initial Potential at −150 mV and Final Potential at −600 mV. The Step was 4 mV, Pulse

Table 2
Time variability of excreted Cu-binding ligands by *Phaeodactylum tricornutum* grown in control (duplicate cultures) and low Cu media (i.e., Cyclam; triplicate cultures). Experimental conditions: pH_F 8.20 ± 0.05; initial [Cu] (i.e. $[Cu]_0$) = $4.4 \cdot 10^{-10}$ mol L^{-1}, and cell densities in the range of 50–80 · 10^3 cell mL^{-1}. $\alpha_{Cu'} = \frac{[Cu']}{[Cu^{2+}]} = 32$, $f_{CuL_i} = [L]_i K'_{Cu'L_i}$.

Treatment	Time H (h)	$[Cu^{2+}]$ (10^{-15} mol L^{-1})	L_1 (10^{-10} mol L^{-1})	L_1 (10^{-19} mol μm^{-2})	log $K'_{Cu'L_1}$	log $K'^{2+}_{Cu'}$	L_2 (10^{-9} mol L^{-1})	L_2 (10^{-19} mol μm^{-2})	log $K'_{Cu'L_2}$	log $K'^{2+}_{Cu'}$	log $f_{Cu'L_1}$
Control	0.04	5.7 ± 0.2	2.0 ± 0.8	0.81 ± 0.3	13.7 ± 0.6	15.2 ± 0.6	1.0 ± 0.2	4.04 ± 0.3	12.3 ± 0.2	13.8 ± 0.2	3.97
	1.22	7.6 ± 0.6	2.3 ± 0.4	0.94 ± 0.1	13.6 ± 0.8	15.1 ± 0.8	1.0 ± 0.2	4.29 ± 0.1	12.1 ± 0.1	13.6 ± 0.1	3.92
	2.17	6.4 ± 0.5	2.4 ± 0.4	0.99 ± 0.1	13.6 ± 0.6	15.1 ± 0.6	1.6 ± 0.2	6.66 ± 0.1	11.9 ± 0.1	13.4 ± 0.1	3.95
	2.2	6.0 ± 0.5	2.9 ± 0.4	1.21 ± 0.2	13.6 ± 0.6	15.1 ± 0.6	1.4 ± 0.2	5.73 ± 0.4	11.9 ± 0.1	13.4 ± 0.1	4.03
	5.79	4.6 ± 0.6	3.1 ± 0.3	1.29 ± 0.1	14.2 ± 0.7	15.7 ± 0.7	1.7 ± 0.7	7.10 ± 0.5	11.5 ± 0.1	13.0 ± 0.1	4.73
	16.65	7.3 ± 0.5	4.2 ± 0.3	1.73 ± 0.3	13.8 ± 0.9	15.3 ± 0.9	1.1 ± 0.6	4.64 ± 0.2	11.8 ± 0.3	13.3 ± 0.3	4.42
	24.14	3.2 ± 0.3	3.6 ± 0.6	1.51 ± 0.2	13.5 ± 0.2	15.0 ± 0.2	1.2 ± 0.1	4.90 ± 0.3	12.2 ± 0.2	13.7 ± 0.2	4.07
	Mean	5.8 ± 1.5	2.9 ± 0.8	1.21 ± 0.3	13.7 ± 0.3	15.2 ± 0.3	1.3 ± 0.3	5.34 ± 1	12.0 ± 0.3	13.5 ± 0.3	4.16 ± 0.3
Cyclam	0.07	2.4 ± 0.2	5.5 ± 0.4	2.08 ± 0.2	13.5 ± 0.1	15.0 ± 0.1	0.9 ± 0.2	3.38 ± 0.8	11.9 ± 0.2	13.4 ± 0.2	4.23
	0.5	3.4 ± 0.3	2.3 ± 0.4	0.87 ± 0.1	14.1 ± 0.2	15.6 ± 0.2	1.1 ± 0.5	4.12 ± 1	12.4 ± 0.2	13.9 ± 0.1	4.41
	1.01	4.4 ± 0.8	3.5 ± 0.3	1.34 ± 0.1	14.3 ± 0.6	15.8 ± 0.6	0.8 ± 0.3	2.91 ± 1	12.0 ± 0.2	13.5 ± 0.2	4.89
	2	3.2 ± 0.9	3.5 ± 0.9	1.32 ± 0.3	13.6 ± 0.8	15.1 ± 0.8	1.5 ± 0.6	5.65 ± 2	12.1 ± 0.3	13.6 ± 0.3	4.1
	5.23	1.9 ± 0.2	6.2 ± 0.6	2.33 ± 0.4	13.4 ± 0.2	14.9 ± 0.2	1.8 ± 0.8	6.69 ± 2	11.9 ± 0.2	13.4 ± 0.2	4.16
	16.83	5.7 ± 0.2	2.6 ± 0.2	0.98 ± 0.1	14.0 ± 0.2	15.3 ± 0.2	1.7 ± 0.6	6.46 ± 2	11.9 ± 0.1	13.4 ± 0.1	4.23
	22.66	3.7 ± 0.2	3.9 ± 0.2	1.49 ± 0.1	14.3 ± 0.1	15.8 ± 0.1	1.5 ± 0.5	5.79 ± 2	12.0 ± 0.2	13.5 ± 0.2	4.84
	23	3.5 ± 0.3	3.0 ± 0.3	1.12 ± 0.1	14.4 ± 0.2	15.9 ± 0.2	1.3 ± 0.3	4.91 ± 1	12.1 ± 0.2	13.6 ± 0.2	4.83
	Mean	3.5 ± 2.0	3.8 ± 1.4	1.55 ± 0.5	13.9 ± 0.4	15.4 ± 0.4	1.3 ± 0.4	4.99 ± 1	12.0 ± 0.2	13.5 ± 0.2	4.46 ± 0.3

Table 3
Cellular Cu adsorption onto cell surface binding sites of *P. tricornutum* after being cultured on two different media, with and without azide (NaN_3) treatment. Note that after the azide addition, only one binding site was detected. Experimental conditions: $pH_F = 8.01 \pm 0.05$, total alkalinity 2400 µmol kg^{-1}, $\alpha_{Cu'} = 20$ (i.e. $\alpha_{Cu'} = [Cu']/[Cu^{2+}]$). Initial Cu concentrations ranged from 0.41 to 29.50 nM. n, number of cultures studied; for the NaN_3 addition treatments, the error displayed is the one associated with the experimental data fitting.

Treatment (n)	Biomass (10^3 cell mL^{-1})	$[\equiv S_1]$ (10^{-19} mol μm^{-2})	$[\equiv S_1]$ (10^{-9} mol L^{-1})	log K'_{ads_1}	log $K'_{ads_1^{Cu^{2+}}}$	log $f_{Cu'S_1}$	$[\equiv S_2]$ (10^{-18} mol μm^{-2})	$[\equiv S_2]$ (10^{-9} mol L^{-1})	log K'_{ads_2}	log $K'_{ads_2^{Cu^{2+}}}$
Control (4)	61 ± 6	5.51 ± 0.2	1.6 ± 0.3	12.93 ± 0.06	14.2 ± 0.1	4.13 ± 0.07	4.93 ± 0.1	14.0 ± 5.4	8.1 ± 0.1	9.4 ± 0.1
Cyclam (3)	71 ± 10	7.85 ± 0.3*	1.8 ± 0.9	12.90 ± 0.04	14.2 ± 0.04	4.16 ± 0.22	6.56 ± 0.2*	21.3 ± 7.0*	7.8 ± 0.1	9.1 ± 0.1
Control-NaN_3 (1)	45 ± 10	–	–	–	–	–	10.6 ± 1	22.5 ± 7.7	7.9 ± 0.1	9.3 ± 0.1
Cyclam-NaN_3 (1)	25 ± 10	–	–	–	–	–	16.2 ± 0.1	14.3 ± 7.4	8.1 ± 0.1	9.5 ± 0.1

* Represent the values that are statistically different ($p < 0.05$) with respect to the Control.

Width of 35 ms, Pulse Period of 200 ms and Pulse Amplitude of 50 mV.

The concentrations of inorganic Cu (Cu′) and Cu-binding ligands (L) in the *filtrate solution* were determined by DPCSV with ligand competition against SA. The *filtrate solution* was split into 20 vials by duplicate (Teflon Savilex vials) with 10 ml each and were spiked with EPPS buffer (final concentration of 0.01 M), Cu additions in the range 0 to 10 nM (1 h equilibrated) and SA (final concentration of 10 µM SA), and equilibrated overnight before analysis (Campos and van den Berg, 1994) (Fig. S1).

The copper speciation in the *filtrate solution* (i.e., the Cu-binding ligands (L_i) and the conditional stability constants (K_{CuLi}) were computed using the ProMCC software (Table 2) (Omanović et al., 2015). Due to the use of EPPS buffer, pH_F for the complexation studies was 8.2 and the side reaction coefficient for Cu ($\alpha = [Cu^{2+}]/[Cu']$ set to 32 (Turner et al., 1981). The ligand type was classified as in Ruacho et al. (2022)

To ensure the absence of natural organic ligands in the UV-irradiated ESTOC seawater, with and without nutrient additions, used in the preparation of the study solution, Cu titrations were also carried out, and no ligands were detected.

2.9. Cell surface Cu-adsorption studies

For the cell surface Cu-adsorption studies, the optimal adsorption time for Cu was first established using kinetic adsorption studies, by characterizing the adsorption of 4.9 ± 0.1 nM Cu as a function of time, ranging from 1 min to 24 h, in nutrient-enriched, UV-irradiated ESTOC seawater at its natural pH_F of 8.01 ± 0.05 (Fig. S2). The biomass for the adsorption studies ranged between 25 and 71 · 10^3 cell mL^{-1}. This experiment established that the required contact time to allow chemical equilibrium between the cell surfaces and the added Cu was 10 min (Fig. S2), as previously described (González-Dávila, 1995).

Once the optimal Cu adsorption time was determined, 20 acid-cleaned Teflon vials with 20 mL of cells in the study solution were prepared. Specific experimental conditions are listed in Table 3. In essence, a specific Cu addition, ranging from 0 (blank, a set of two) to ~29 nM, was made to each vial, and was allowed to equilibrate for 10 ± 0.1 min at room temperature (20 ± 0.2 °C). After this 10 min contact time, the cells were removed from the study solution using a 0.45 μm pore-size filter (acid-clean nitrocellulose filter, Sarthorius™). After filtration, the adsorbed Cu onto cell surfaces (Cu^{ads}) was determined from the difference between the Cu concentration added to the solution (plus the initial background Cu in the seawater) (i.e., $Cu_{T,add}$) and the Cu concentration in solution after the cells were removed (Cu^{ads}_{sol}) (i.e., $Cu_{T,add} - Cu^{ads}_{sol} = Cu^{ads}$). Cu^{ads}_{sol} may also contain ligands excreted by the cells during the experiment, such that $\left[Cu^{ads}_{sol}\right] = [Cu'] + \sum[CuL_i]$. Therefore, before determining Cu^{ads}_{sol}, the samples were UV-irradiating for 4 h to destroy the organic ligands. These Cu-binding ligands excreted by the cells during the adsorption experiments were also measured, as these excreted ligands may compete for Cu with Cu-binding sites at the cell surface.

2.10. Characterizing reductase activity at the cell surface Cu-binding sites

To investigate the reductase activity at the Cu-binding sites, a set of Cu adsorption studies were done with *P. tricornutum*, after exposure to 0.01 M sodium azide (NaN_3, Sigma-Aldrich Reagent Plus) (Martinez et al., 2008) for 60 min. The cells were washed 5 times with UV-irradiated seawater to remove any excess of azide, before the Cu adsorption capacity determinations.

2.11. Candidate genes and sequence analysis

Genes potentially involved in Cu transport (Table 4) were identified in the *P. tricornutum* (CCAP1005) genome (JGI; https://mycocosm.jgi.doe.gov/Phatr2/Phatr2.home.html) by blastp searches using homologous genes from the yeast and the marine diatom *T. pseudonana* (CCMP 1335) and *T. oceanica* (CCMP 1005). They included members of the CTR family, ferric reductases (FRE1, FRE2), the NRAMP and genes of the ZIP family (Kustka et al., 2007; Guo et al., 2015; Kong and Price, 2019, 2022a).

The conserved motifs of *Pt*CTR N-terminus were analyzed by comparing its protein sequence with homologs from CTRs of *H. sapiens* (*h*CTR1: AAB66306) and *T. oceanica* CCMP1005 (*To*CTR3a: EJK74005), for which the functions on Cu transport were confirmed by the yeast complementation assays (Kong and Price, 2019; Kar et al., 2022). Multiple alignments were performed with Clustal Omega (http://www.ebi.ac.uk/Tools/msa/clustalo/; Sievers et al., 2011).

2.12. Computation of the binding properties of cell surface Cu adsorption sites

During the adsorption experiments, the total dissolved Cu ($Cu_{T,add}$, which includes the background Cu concentration and the added Cu) may be distributed between inorganic and organic ligands in solution and on the cell surface,

Table 4
Gene list of potential Cu transporters and its associated reductases in three model diatoms. Genes potentially involved in Cu transport were identified in the *P. tricornutum* genome (JGI; https://mycocosm.jgi.doe.gov/Phatr2/Phatr2.home.html) by blastp searches using homologs of Cu transporters and reductases identified in *S. cerevisiae*, *T. pseudonana*, and *T. oceanica* (Dancis et al., 1994; Larimer et al., 2004; Guo et al., 2015; and Kong and Price, 2019, 2022a). The *P. tricornutum* CCAP1055/1 clone represents a monoclonal culture derived from a fusiform cell in May 2003 from strain CCMP632, which was originally isolated in 1956 off Blackpool (U.K.). For ZIP, we identified 10 ZIPs in the *P. tricornutum* genome, 8 ZIPs in *T. oceanica* 1005 genome and 8 ZIPs in the *T. pseudonana* genome. Here we only list the *Pt*ZIPs that are homologs of *Tp*ZIP268980, which was down-regulated under low Cu growth conditions, and *Tp*ZIP32375, which was upregulated when Cu-limited cells were exposed to a Cu addition (Guo et al., 2015). The genes identified in previous studies as most likely to be linked to Cu transport are highlighted in bold.

Genes	*P. tricornutum* CCAP1055/1	*T. pseudonana* CCMP1335	*T. oceanica* CCMP1005
High affinity copper Transporters (CTRs)	***Pt*CTR (49224*)**	***Tp*CTR (24275)**	*To*CTR1 (31553)
	*Pt*CTR (47805)	***Tp*CTR (9391)**	*To*CTR2 (30982)
	*Pt*CTR (48793)		***To*CTR3a (04344)**
			***To*CTR3b (17625)**
Ferric reductases (FREs)	***Pt*FRE1 (54486)**	*Tp*FRE1 (11375)	***To*FRE1 (06605)**
	***Pt*FRE2 (46928)**	***Tp*FRE2 (3129)**	***To*FRE2 (13522)**
	*Pt*FRE3 (54940)		*To*FRE3 (27289)
	*Pt*FRE4 (54409)		*To*FRE4 (20372)
	*Pt*FRE5 (54982)		
Natural resistance-associated macrophage protein (NRAMP)	No hit	***Tp*NRAMP (9840)**	*To*NRAMP (00493)
Zrt/IRT-like proteins (ZIPs)	***Pt*ZIP (49400)**	***Tp*ZIP (268980)**	*To*ZIP (01483)
	*Pt*ZIP (26405)	***Tp*ZIP (32375)**	*To*ZIP (16050)
	*Pt*ZIP (38445)		*To*ZIP (16051)
	*Pt*ZIP (52343)		*To*ZIP (22051)
	*Pt*ZIP (22166)		*To*ZIP (24780)

* Protein ID

$$\left[Cu_{T,add}\right] = [Cu'] + [CuL_1] + [CuL_2] + \sum\nolimits_i [\equiv S_iCu] \cdot \left(\frac{\text{no.cell}}{L}\right) \quad (1)$$

where Cu′ represents the inorganic Cu concentration (mol L^{-1}); CuL_1 and CuL_2 (mol L^{-1}) represent the Cu bound by dissolved organic ligands L_1 and L_2 produced by the phytoplankton (at least two types of ligands were considered) and $\equiv S_iCu$ was the Cu bound to any cell surface Cu binding sites (mol $cell^{-1}$), converted to mol L^{-1} after multiplying by the cell number in each study (cell L^{-1}). The corresponding conditional complexation constants for the dissolve (L_i) and the cell surface ($\equiv S_i$, after in expressed as S_i) binding sites (for simplicity expressed as K for the inorganic Cu) are:

$$Cu' + L_1 \leftrightarrow CuL_1 \; K_{CuL_1} = \frac{[CuL_1]}{[Cu'][L_1]}; \text{in } \left(\frac{L}{\text{mol}}\right) \quad (2)$$

$$Cu' + L_2 \leftrightarrow CuL_2 \; K_{CuL_2} = \frac{[CuL_2]}{[Cu'][L_2]}; \text{in } \left(\frac{L}{\text{mol}}\right) \quad (3)$$

$$Cu' + S_1 \leftrightarrow S_1Cu\ K_{ads_1} = \frac{[S_1Cu]}{[Cu'][S_1]}; \text{in } \frac{\left(\frac{mol}{cell}\right)}{\left(\frac{mol}{L}\right)\left(\frac{mol}{cell}\right)} = \left(\frac{L}{mol}\right) \quad (4)$$

$$Cu' + S_2 \leftrightarrow S_2Cu\ K_{ads_2} = \frac{[S_2Cu]}{[Cu'][S_2]}; \text{in } \frac{\left(\frac{mol}{cell}\right)}{\left(\frac{mol}{L}\right)\left(\frac{mol}{cell}\right)} = \left(\frac{L}{mol}\right) \quad (5)$$

Two types of cell surface Cu binding sites were also assumed. The total ligand concentration, L_T, able to complex Cu in solution and on the cell surface, was calculated using:

$$\begin{aligned}[L_T] &= [L_{T1}] + [L_{T2}] + [S_T] \\ &= [L_1] + [CuL_1] + [L_2] + [CuL_2] + [S_1] + [S_1Cu] + [S_2] + [S_2Cu]\end{aligned} \quad (6)$$

The total cell surface Cu binding sites, $[S_T]$, was determined as:

$$\begin{aligned}[S_T] &= [S_1] + [S_1Cu] + [S_2] + [S_2Cu] \\ &= [S_1] + K_{ads_1}Cu[S_1] + [S_2] + K_{ads_2}Cu[S_2] \\ &= [S_1](1 + K_{ads_1}Cu) + [S_2](1 + K_{ads_2}Cu)[\equiv S_T] = [\equiv S_1] + [\\ &\equiv S_1Cu'] + [\equiv S_2] + [\equiv S_2Cu'] = [\equiv S_1] + K'_{ads_1}Cu'[\equiv S_1] + [\\ &\equiv S_2] + K'_{ads_2}Cu'[\equiv S_2] = [\equiv S_1]\left(1 + K'_{ads_1}Cu'\right) + [\\ &\equiv S_2]\left(1 + K'_{ads_2}Cu'\right)\end{aligned} \quad (7)$$

In the excreted Cu binding ligands studies, the data treated using the ProMCC software allowed to compute the complexing properties ($[L_{T1}]$, $[L_{T2}]$, K_{CuL_1}, K_{CuL_2} and $[L_1]$ and $[L_2]$) and Cu speciation in the solution ($[Cu^{2+}]$, $[Cu']$and $[CuL_1]$ and $[CuL_2]$).

When the adsorption studies were carried out, the total Cu ($[Cu_{T,add}]$) was known, and that in solution after 10 min adsorption equilibration ($[Cu^{ads}_{sol}]$) (i.e., $[Cu^{ads}_{sol}] = [Cu'] + [CuL_1] + [CuL_2]$) was determined in the UV-irradiated solution. The three components of Cu^{ads}_{sol} and the bindings constants of the cell surface Cu binding sites were computed considering the competition between the dissolved ligands and cell surface binding sites, using a custom MATLAB iterative routine. In a first approximation, it was assumed that $K_{ads_2} < K_{ads_1} \ll K_{CuL_2} < K_{CuL_1}$ and, therefore the cell surface Cu adsorption did not significantly affect the equilibria between Cu and the excreted dissolved ligands, so that

$$\begin{aligned}[Cu^{ads}_{sol}] &= [Cu'] + [CuL_1] + [CuL_2] = [Cu'] + K_{CuL_1}\cdot[Cu']\cdot[L_1] + K_{CuL_2}\cdot[Cu']\cdot[L_2] \\ &= [Cu'](1 + K_{CuL_1}\cdot[L_1] + K_{CuL_2}\cdot[L_2])\end{aligned} \quad (8)$$

where, for excreted dissolved ligand type 1

$$[L_1] = \frac{[L_{T1}]}{1 + K_{CuL_1}\cdot[Cu']} \quad (9)$$

and

$$[CuL_1] = K_{CuL_1}\cdot[Cu']\cdot[L_1] \quad (10)$$

For the excreted dissolved ligand type 2,

$$[L_2] = \frac{[L_{T2}]}{1 + K_{CuL_2}\cdot[Cu']} \quad (11)$$

and

$$[CuL_2] = K_{CuL_2}\cdot[Cu']\cdot[L_2] \quad (12)$$

Therefore,

$$[Cu'] = \frac{[Cu^{ads}_{sol}]}{1 + \frac{K_{CuL_1}[L_{T1}]}{1+K_{CuL_1}[Cu']} + \frac{K_{CuL_2}[L_{T2}]}{1+K_{CuL_2}[Cu']}} \quad (13)$$

In order to compute $[Cu']$ in equilibrium with the adsorbed Cu, ($[Cu_{T,add}] - [Cu^{ads}_{sol}]$), an iterative procedure was performed assuming as a first step that $[Cu'] = [Cu^{ads}_{sol}]$. Then, a Scatchard and van den Berg/Ruzic plot (Laglera-Baquer et al., 2001) was applied and the corresponding adsorption variables for each of the possible data distributions at the pH of the solution were computed.

$$\frac{[SCu]}{[Cu']} = -K_{ads}\cdot[SCu] + [S]\cdot K_{ads} \quad (14)$$

$$\frac{[Cu']}{[SCu]} = \frac{[Cu']}{[S]} + \frac{1}{K_{ads}\cdot[S]} \quad (15)$$

It was determined that $K_{ads_2} \ll K_{CuL_2} < K_{ads_1} < K_{CuL_1}$. The constants of the cell surface Cu binding sites were thus included in a new iterative procedure.

$$[Cu'] = \frac{[Cu^{ads}_{sol}]}{1 + \frac{K_{CuL_1}[L_{T1}]}{1+K_{CuL_1}[Cu']} + \frac{K_{CuL_2}[L_{T2}]}{1+K_{CuL_2}[Cu']} + \frac{K_{ads_1}[S_1]}{1+K_{ads_1}[Cu']} + \frac{K_{ads_2}[S_2]}{1+K_{ads_2}[Cu']}} \quad (16)$$

where the new $[Cu']$ was used in the Scatchard plot to recalculate new cell surface Cu binding sites parameters until the values converged (better than 0.1 %).

2.13. Statistical analysis

The results of the Cyclam treatment were compared with those of the control using a two-sample Student's *t*-test. Following Semeniuk et al. (2015) and Winter (2013), Type I (false positives) can be considered when the two-way *t*-test is applied to a limited dataset with non-normal distributions. Type II errors (false negatives) can only be detected when the mean values are high. Considering the lack of Student's t-distribution for the current dataset, the statistical analysis of these data is limited and can only be used to distinguish relatively large differences between mean values that would be statistically significant for $p < 0.05$. The statistical analysis was carried out using the software Past version 3.15.

3. Results

3.1. Growth rate

The acclimation of *P. tricornutum* to the two growth conditions considered, control (CO_{MEDIUM}) and low Cu availability (Cy_{MEDIUM}), was monitored before the excreted Cu-binding ligands studies and the cell surface Cu-binding site studies. The exponential absolute growth rates μ (d^{-1}) obtained for these cultures were very similar, ranging between 0.94 and 1.03 d^{-1} (Table S2). In the fully enriched f/2 media, the growth rate achieved by *P. tricornutum* was usually faster (1.72 d^{-1}). The surface area of *P. tricornutum* grown under control was significantly higher than in low Cu conditions (Table S2).

3.2. Cu uptake kinetics of P. tricornutum

Fourteen Cu concentrations, ranging from 2 to 2000 nM, were used in the Cu uptake kinetics experiments. For each concentration, cellular Cu accumulation (zmol μm^{-2}) increased linearly as a function of time in the course of approximately 2.5 h. The rates of Cu uptake as a function of Cu concentrations exhibited biphasic Michaelis–Menten uptake kinetics. The first phase was observed at low Cu concentrations (0–300 nM), while the second one was observed at higher Cu concentrations (up to 2000 nM) (Fig. 1). This biphasic uptake saturation kinetic pattern was assumed to reflect the simultaneous operation of a high- and a low-

affinity uptake system at low and high Cu concentrations, respectively (Knauer et al., 1997), as previously observed for two other marine diatoms, *T. oceanica* and *T. pseudonana* (Guo et al., 2010).

The maximum rates of Cu uptake (V_{max}) of the low and high-affinity Cu transport systems differed by approximately 13-fold and were 19.26 ± 10.6 and 1.48 ± 0.6 zmol μm^{-2} h^{-1}, respectively (Table 1). The half-saturation constant (K_m) of the high-affinity uptake system (0.08 ± 0.07 pM Cu′) was ~17-fold lower than that of the low-affinity Cu transport system (1.37 ± 1.12 pM Cu′).

3.3. Cu-binding properties of the P. tricornutum exudates

Cultures of *P. tricornutum*, grown in the control and low Cu conditions, were allowed to excrete Cu-binding ligands for various time intervals, ranging from 3 min to 24 h (Table 2). The excreted ligands were investigated using voltammetry at pH_F 8.2 ± 0.05 (buffered ESTOC seawater) and in the presence of background Cu concentrations ($[Cu]_0 = 4.41 \cdot 10^{-10}$ mol L^{-1}) (Fig. 2, Table 2). Regardless of excretion time, the L_1 concentrations were practically constant for cells acclimated to both culture conditions, with mean values of $2.9 \pm 0.8 \cdot 10^{-10}$ (CO_{MEDIUM}) and $3.8 \pm 1.3 \cdot 10^{-10}$ (Cy_{MEDIUM}) mol L^{-1} and with a mean log K_{CuL_1} of 13.7 ± 0.3 and 13.9 ± 0.4, respectively. When expressed as log $K_{Cu^{2+}L_1}$ (Table 2), L_1 ligands correspond with the highest strength ligands range defined in Ruacho et al. (2022). The concentrations of L_2 ligands excreted by the cells were one order of magnitude higher than those of L_1, with mean concentrations of $1.3 \pm 0.3 \cdot 10^{-9}$, and $1.3 \pm 0.4 \cdot 10^{-9}$ mol L^{-1} and log $K_{CuL_2}K'_{CuL_2}$ of 12.0 ± 0.3 and 12.0 ± 0.2 for the control and low Cu availability media, respectively. No statistical differences among the treatments or time intervals within treatments were found. The latter results (Table 2) indicate that the ligands were excreted by the cells within 3 min (0.04 h) in the *study solution* and remained steady for the duration of our measurements (i.e., 24 h).

The estimated concentrations of free Cu (i.e. $[Cu^{2+}]$) did not vary significantly between the treatments, averaging $5.8 \pm 1.5 \cdot 10^{-15}$ and $3.5 \pm 2.0 \cdot 10^{-15}$ mol Cu^{2+} L^{-1} for the cells acclimated to the control and low Cu availability media, respectively. This indicates that the Cu-binding ligands excreted by *P. tricornutum* acclimated to low Cu are very similar to those of the control and would have a similar effect on Cu speciation.

Note that since the seawater was UV-irradiated and the phytoplankton were rinsed with organic-free seawater, the ligands determined in these studies correspond to those excreted by the phytoplankton. Moreover, due to the fact that to achieve maximum sensitivity (Campos and van den Berg, 1994), the voltametric ligand titration method is done at pH_F 8.2 rather than at ambient ESTOC pH_F 8.01 ± 0.05, the $[Cu^{2+}]$ in the ambient ESTOC seawater - assuming the organic to inorganic ligands ratio remains constant- should increase to $9.3 \pm 2.4 \cdot 10^{-15}$ and $5.6 \pm 3.2 \cdot 10^{-15}$ mol Cu^{2+} L^{-1}.

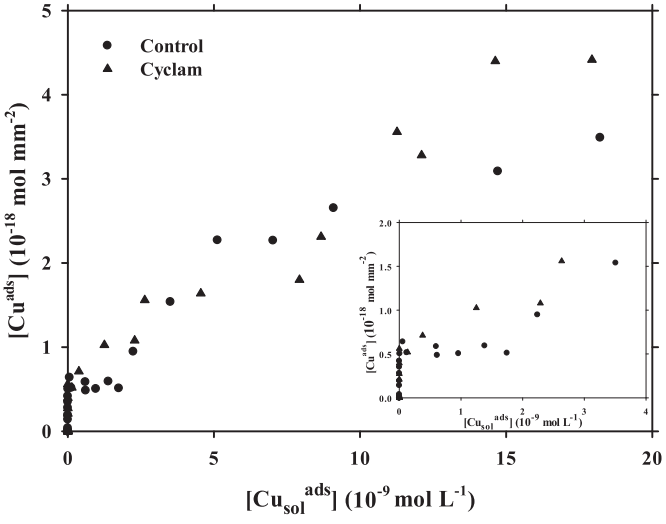

Fig. 2. Cellular Cu adsorption onto cell surface binding sites of *P. tricornutum*, grown in control and low Cu media (i.e., Cyclam) as a function of the remaining Cu concentration in solution, after Cu additions ranging between 0 and 29 nM, at constant $pH_F = 8.01 \pm 0.05$. The insert plot represents the adsorption when the remaining Cu concentration was <4 nM.

3.4. Kinetic studies of Cu-binding sites at the cell surface

Copper sorption kinetics were carried out to provide a quantitative characterization of the Cu-binding capacity of the cell surface of *P. tricornutum*, after growing in the control and low Cu media. The percentage of Cu sorbed onto *P. tricornutum* as a function of time, during 280 min, in the presence of a total Cu concentration of $4.87 \cdot 10^{-9}$ mol L^{-1} (i.e., added $4.43 \cdot 10^{-9}$ mol L^{-1} + initial [Cu] of $4.4 \cdot 10^{-10}$ mol L^{-1}) ranged between 20 and 60 % (Fig. S2). Like previous observations with higher Cu concentrations (at μM levels; Gonzalez-Davila et al., 1995), most of the Cu (about 55 % of the total added) was adsorbed within the first 10 min of equilibration time. After this 10 min (Fig. S2), the sorbed Cu onto the cell surface increased slightly due to membrane diffusion-uptake processes (González-Dávila, 1995). Therefore, 10 min contact time was used in all the adsorption studies. Using the fastest V_{max} from the *P. tricornutum* Cu uptake experiments ($19.3 \cdot 10^{-21}$ mol Cu μm^{-2} h^{-1}, Table 1) and the cell density in the sorption experiments (Table 3), we calculated that the maximum % of the absorbed Cu due to uptake in the first 10 min was 0.1 %.

3.5. Characterizing Cu-binding sites at the cell surface of P. tricornutum

The cell surface Cu-binding sites were measured at Cu concentrations ranging from ~0–30 nM, which are much lower than previous studies (i.e., >100 nM; Gonzalez-Davila et al., 1995) (Fig. 2; Table 3). In the presence of these low Cu concentrations and these experimental conditions, (i.e., *study solution* with 0.45 nM Cu, and the cells and their excreted dissolved Cu-binding ligands), a competition for Cu between the high-affinity ligands in solution and the Cu-binding groups at the cell surface is expected to occur.

The shape of the adsorption curves (Fig. 2) was biphasic, unlike those in previous phytoplankton adsorption studies (González-Dávila, 1995), which exhibited a monophasic hyperbola. The curves identified two types of adsorption sites at the cell surface. An iterative MATLAB routine (see methods) was applied to compute the concentrations of Cu-binding ligands at the cell surface (S_1 and S_2, Table 3) after accounting for the excreted Cu binding ligands in solution (L_1 and L_2, Table 2), as well as their respective complexing properties. The results indicate that the algal surface properties presented two types of Cu-binging sites, with *log* K_{ads_1} and *log*K_{ads_2} for the control cultures ranging from 12.93 ± 0.06 to 8.1 ± 0.1 for the high- and low-affinity cell surface Cu-binding sites, respectively (Table 3). Furthermore, the density of these two types of Cu-binding cell surface sites for the control cultures differed by an order of magnitude, with an average surface density of $5.51 \pm 0.2 \cdot 10^{-19}$ and $4.93 \pm 0.1 \cdot 10^{-18}$ mol μm^{-2} for the high- and low-affinity sites, respectively.

In addition, the properties of the Cu binding sites at the cell surface of *P. tricornutum* grown under control versus low-Cu conditions were different. For example, the density of the high-affinity adsorption sites on the cell surface (Table 3) was significantly higher for the cells grown in the low Cu treatment relative to the control (7.85 ± 0.3 vs. $5.51 \pm 0.2 \cdot 10^{-19}$ mol μm^{-2}, respectively). Similarly, for the low-affinity adsorption sites, the cells grown under low Cu had a significantly higher density than those in the control treatment (6.56 ± 0.2 vs. $4.93 \pm 0.1 \cdot 10^{-18}$ mol μm^{-2}, respectively). In contrast, neither the affinity constant of the high- nor the low-affinity adsorption sites significantly differed between the two growth treatments.

To determine the biotic or abiotic nature of Cu-binding sites at the cell surface of *P. tricornutum*, additional measurements were done in the presence of azide-treated algal cells (Table 3). Azide inhibits electron transport activity (Anderson and Morel, 1982; Martinez et al., 2008). Thus, if a reductive step is involved in Cu-binding and/or transport, the Cu-binding site would be inhibited in the presence of azide. After the addition of azide, only the low-affinity cell surface sites (i.e., average density of $18.4 \cdot 10^{-9}$ mol L^{-1}, and $log K_{ads_2}$ $log K^{Cu^{2+}}_{ads,2}$ of 8.0 ± 0.1) remained active.

3.6. Comparing high-affinity Cu-binding sites at the cell surface of *P. tricornutum* vs. high-affinity ligands released into solution by *P. tricornutum*

The high-affinity Cu-binding sites at the cell surface of *P. tricornutum* present similar affinity constants under the two growth conditions, with an average $log K_{ads_1}$ of 12.9 ± 0.1 (Table 3). These constants were between the high- and low-affinity constants for the ligands excreted by *P. tricornutum* in solution (Table 2). When the concentrations of Cu-binding sites were normalized to cell densities (i.e., expressed as mol L^{-1}), the concentration of the high-affinity Cu-binding sites on the cell surface ($1.6–1.8 \cdot 10^{-9}$ mol L^{-1}; Table 3) were one order of magnitude higher than those high-affinity ligands released into solution by *P. tricornutum* ($2.9–3.8 \cdot 10^{-10}$ mol L^{-1}; Table 2).

Using the voltammetric kinetic measurements and a theoretical kinetic model (i.e., $Cu' + L_i \leftrightarrow CuL_i$ or $Cu' + S_i \leftrightarrow CuS_i$)—solved by the Gepasi software (Mendes, 1997)—we calculated the forward and dissociation rate constants of these high-affinity Cu-binding sites at the cell surface and those released by *P. tricornutum* (i.e., S_1 vs. L_1; Table 5). The highest forward rate constants, with respect to Cu', were observed for the ligands released into solution (i.e., ranging from 6.0 to $8.81 \cdot 10^8$ M^{-1} s^{-1} for Cu'), relative to the high-affinity Cu binding sites (i.e., ranging from 1.10 to $1.20 \cdot 10^7$ M^{-1} s^{-1} for Cu'). In contrast, the dissociation rate constants were faster for the high-affinity, cell surface Cu binding sites S_1 ($\sim 1.33 \cdot 10^{-6}$ s^{-1} for Cu') than the high-affinity L_1 ligands released by *P. tricornutum* ($0.88–1.19 \cdot 10^{-5}$ s^{-1} for Cu').

4. Discussion

Marine phytoplankton can release strong organic complexes for Cu to lower toxicity (Coale and Bruland, 1988; Moffett and Brand, 1996; Echeveste et al., 2018; Gordon et al., 2000; Croot et al., 2000). Diatoms have been shown to take up Cu via low and high-affinity transport systems (Guo et al., 2010; Kong and Price, 2019). In this study, using a combination of voltammetric measurements and physiological studies, we characterized the Cu uptake kinetics of *P. tricornutum*, identified the putative genes involved in the low- and high-affinity Cu transport systems (Table 4), as well as determined the complexing properties of strong organic Cu ligands released by *P. tricornutum* (Table 2), and Cu-binding sites at its cell surface (Table 3). These data were then combined to determine the formation rate constants of the Cu transporters at the cell surface of *P. tricornutum*, as well as the internalization rate constant of Cu transport. The data were compared with those for Fe transport in the centric diatom, *T. weissflogii*. Furthermore, the relationship between the concentrations of essential inorganic trace metals in oceanic surface waters and the complexation rate constants (k_f) of the respective trace metal transporter sites on the cell surface of marine diatoms was revisited.

4.1. Growth rates of *P. tricornutum* in enriched, natural North Atlantic seawater

The *P. tricornutum* cells were grown in macronutrients and vitamins-enriched natural N. Atlantic seawater (ESTOC) collected in the oligotrophic waters off the coast of the Canary Islands. In the low Cu treatment, the growth rate of *P. tricornutum* was not significantly slower than that in the control treatment, but the cellular surface area was significantly smaller. Interestingly, the *P. tricornutum* growth rates in the control and the Cyclam treatments were significantly slower than those in regular f/2 medium (i.e., with additions of macronutrients, vitamins and all essential metals: Cu, Co, Mn, Mo, Zn, and Fe bound to 10 μM EDTA). Even though the concentrations of trace metals in the ESTOC seawater were relatively low (Table S1), our study aimed to investigate the physiology of *P. tricornutum* in natural trace metal oceanic conditions; thus, we purposely did not add any metals or EDTA.

Marine diatoms may change their physiology and transcriptome before their growth rates are affected by low Cu conditions (Kim and Price, 2017; Kong and Price, 2022a). So, similarly, even though there were no significant differences in growth rates between the control and the low Cu *P. tricornutum* cultures. The 25 % reduction in cell surface area and the voltammetric measurements suggest a series of physiological adaptations to low Cu availability in *P. tricornutum.* For example, the density of the high-affinity Cu-binding sites at its cell surface was 1.4 times higher in cells grown with low Cu than those of the control. Therefore, in the discussion below we assume that *P. tricornutum* was Cu-stressed, but not Cu-limited.

4.2. Copper uptake kinetics of *P. tricornutum*

The biphasic Cu uptake saturation kinetic pattern was assumed to reflect the simultaneous operation of a high- and a low-affinity uptake system (Knauer et al., 1997), as previously observed for two other marine diatoms, *T. oceanica* and *T. pseudonana* (Guo et al., 2010; Kong, 2022).

Careful examination of the data indicates that between 700 and 1000 nM Cu, there is a large increase in Cu uptake, which then quickly plateaus. In our previous investigation with *T. pseudonana* (Guo et al., 2010), a sharp increase in Cu uptake was also noted between 700 and 1000 nM Cu (see Fig. 1, in Guo et al., 2010), so there might be a threshold Cu concentration at which phytoplankton are unable to properly control the influx of Cu into the cell, and thus Cu uptake continues to increase and does not saturate. We actually observed this for the low-affinity Cu transport system of *T. pseudonana* (a coastal diatom)

Table 5
Formation and dissociation rate constants of the excreted Cu-organic ligands (i.e., L_1 and L_2) and surface Cu-binding sites (i.e., S_1 and S_2), computed using the voltammetric measurements and a theoretical kinetic model (i.e., $Cu' + L_i \leftrightarrow Cu'L_i$ or $Cu' + S_i \leftrightarrow Cu'S_i$)—solved by the Gepasi software.[#]

Media	Cu-binding ligands excreted		Surface Cu-binding sites		Cu-binding ligands		Surface Cu-binding sites	
	k_f M^{-1} s^{-1} (Cu′)		k_f M^{-1} s^{-1} (Cu′)		k_d s^{-1} (Cu′)		k_d s^{-1} (Cu′)	
	L_1	L_2	S_1	S_2	L_1	L_2	S_1	S_2
Control	$6.0 \cdot 10^8$	$8.81 \cdot 10^8$	$1.20 \cdot 10^7$	$4.75 \cdot 10^5$	$1.19 \cdot 10^{-5}$	$8.70 \cdot 10^{-4}$	$1.30 \cdot 10^{-6}$	$7.30 \cdot 10^{-3}$
Cyclam	$7.1 \cdot 10^8$	$8.81 \cdot 10^8$	$1.10 \cdot 10^7$	$3.01 \cdot 10^5$	$8.80 \cdot 10^{-6}$	$8.70 \cdot 10^{-4}$	$1.35 \cdot 10^{-6}$	$4.50 \cdot 10^{-3}$
Average	$\mathbf{6.58 \cdot 10^8}$	$\mathbf{8.81 \cdot 10^8}$	$\mathbf{1.15 \cdot 10^7}$	$\mathbf{3.88 \cdot 10^5}$	$\mathbf{1.04 \cdot 10^{-5}}$	$\mathbf{8.70 \cdot 10^{-4}}$	$\mathbf{1.33 \cdot 10^{-6}}$	$\mathbf{5.90 \cdot 10^{-3}}$
SD	$7.35 \cdot 10^7$	$1.41 \cdot 10^5$	$7.07 \cdot 10^5$	$1.23 \cdot 10^5$	$2.19 \cdot 10^{-6}$	$1.41 \cdot 10^{-7}$	$3.54 \cdot 10^{-8}$	$1.98 \cdot 10^{-3}$

Average values are shown in bold for easier visualization.
[#] Gepasi software (version 3.30; Mendes, 1997) is a simulation of biochemical reactions and allows the introduction of kinetics and equilibrium reactions.

grown under Fe replete conditions, in the presence of low or high Cu concentrations (see Table 3, in Guo et al., 2010); but not for *T. oceanica* (and oceanic diatom). Further studies are needed.

The maximum rates of Cu uptake (V_{max}) of the low and high-affinity Cu transport systems in *P. tricornutum* differed by approximately 13-fold (Tables 1 and 6). The half-saturation constant (K_m) of the high-affinity uptake system (0.08 ± 0.07 pM Cu′) was ~17-fold lower than that of the low-affinity Cu transport system (1.37 ± 1.12 pM Cu′). The high-affinity K_m of *P. tricornutum* was like that of the oceanic centric diatoms *T. oceanica* (0.08 pM Cu′) and 8-fold lower than that of the coastal diatom *T. pseudonana* (0.64 pM Cu′) (Table S3). *P. tricornutum* is an important model organism for studying Fe acquisition and homeostasis mechanisms in eukaryotic phytoplankton (reviewed by Sutak et al., 2020), and is well adapted to low Fe conditions (Kustka et al., 2007). So, it is possible that *P. tricornutum* also easily adapts to low Cu conditions.

The genes potentially involved in Cu transport and homeostasis in marine diatoms have been identified in the genome of coastal *T. pseudonana* (CCMP1335; Guo et al., 2015) and the oceanic *T. oceanica* (CCMP1005; Kong and Price, 2019). Thus, to identify the high- and low-affinity Cu transporters in *P. tricornutum*, we searched the only sequenced genome of *P. tricornutum* (CCAP1005) for homologs of the components of the high-affinity Cu transport system (i.e., the high-affinity Cu^+ transporter, CTR; and the ferric reductases, FRE), as well as two putative, low-affinity Cu^{2+} transporters (i.e., NRAMP and ZIPs), and compared the results to those in *T. oceanica* and *T. pseudonana* (Table 4).

In the sequenced genome of *P. tricornutum*, we identified three candidate genes for the high-affinity Cu^+ transporter CTR, as well as five ferric reductase FRE (Table 4). Kustka et al. (2007) first identified *P. tricornutum*, *Pt*FRE1 and 2, as having the conserved required motifs and secondary structure of NADPH-transmembrane oxidoreductases in other model organisms, including *Saccharomyces cerevisiae*, *Arabidopsis thaliana*, and *Homo sapiens*; and *Pt*FRE1 and 2 have been suggested to be involved in the enzymatic reduction of Fe^{3+} during Fe uptake (Kustka et al., 2007; Allen et al., 2008 reviewed by Sutak et al., 2020). Similarly, *Tp*FRE2 (Guo et al., 2015) and *To*FRE1 and 2 (Kong and Price, 2022a, 2022b) were suggested to be involved in Cu^{2+} reduction, and the high-affinity Cu transport systems. In addition, ten ZIP-like proteins were identified in the genome of *P. tricornutum* (CCAP1005), which transport a variety of divalent metals, including Cu^{2+} (Ajeesh Krishna et al., 2020). One of these ZIPs, *Pt*ZIP49400 is a homolog of *Tp*ZIP268980 ((Table 4), which was suggested to be the potential low-affinity Cu^{2+} transporter, given its downregulation in Cu-limited *T. pseudonana* (Guo et al., 2015).

Surprisingly, in the genome of *P. tricornutum* we could not identify homologs of NRAMP, another divalent, non-specific metal transporter (Table 4), found in *T. oceanica* and *T. pseudonana* (Kustka et al., 2007; Guo et al., 2015; Kong and Price, 2022a).

Of the three putative high-affinity Cu^+ transporters (*Pt*CTR) identified in the *P. tricornutum* genome, *Pt*CTR(49224) exhibits the greatest similarity to *T. oceanica To*CTR3a, identified as a high-affinity Cu transporter in *T. oceanica* (Kong and Price, 2019) (Table 4). Furthermore, *P. tricornutum* (*Pt*CTR_49224: EEC44514) and *T. oceanica* CCMP1005 (*To*CTR3a: EJK74005) have the conserved motifs of the N-terminus of the CTR protein in *H. sapiens* (*h*CTR1: AAB66306), which has been studied in great detail (see below, Kar et al., 2022; Janoš et al., 2022).

4.3. Cu-binding properties of the *P. tricornutum* exudates released in the presence of environmentally relevant, dissolved Cu concentrations

P. tricornutum is known for releasing organic ligands to complex Cu (Zhou and Wangersky, 1989; Croot et al., 2000). Thus, we aimed to investigate whether *P. tricornutum* exudates strong organic Cu complexes when dissolved Cu concentrations are as low as those in the open ocean (i.e., <0.5 nM, (Coale and Bruland, 1990; Sunda et al., 1990). To do these measurements, we resuspended *P. tricornutum,* once acclimated to control and low Cu culture conditions, in UV-irradiated and sterilized ESTOC seawater, where we then determined the concentrations and stability constants of Cu-binding ligands excreted by *P. tricornutum* as a function of time, in the course of a day. During this time, the L_1 concentrations and conditional stability constant did not vary significantly between the control and the low Cu culture treatments. This indicates that the strong organic Cu-binding ligands excreted by *P. tricornutum* acclimated to low Cu levels are very similar to those of the control and would have a similar effect on Cu speciation. The concentrations of L_2 ligands excreted by the cells were one order of magnitude higher than those of L_1, with almost identical Log K_{CuL_2} (Table 2).

Furthermore, the fact that *P. tricornutum* cells generated two strong soluble Cu-binding ligand types (i.e., ~0.35 nM L_1 and 1.3 nM L_2) within 4 min in the new *study solution*, UV-irradiated seawater, despite its low Cu concentration (0.44 nM Cu) was very surprising. At present, we do not know the specific function of these strong organic Cu ligands released by *P. tricornutum*. They may be released to enhance Cu uptake, either via a) direct uptake by the high-affinity Cu transport system, which involves Cu^{2+} bound to organic complexes, a reductive step and Cu^+ internalization, or b) indirect ligand-exchange shuttle mechanism with low-affinity Cu transporter, as suggested by Semeniuk et al. (2015) for indigenous phytoplankton in the NE Pacific Ocean. Indeed, the quantity of excreted ligands was high enough to buffer free Cu concentrations to very low levels (i.e., pCu = −log [Cu^{2+}], from 14.23 to 14.45), which have been shown to limit the growth of other coastal diatoms (Annett et al., 2008).

Table 6
Kinetic parameters of Cu transport in *Phaeodactylum tricornutum* grown in low Cu conditions (this study), and of Fe transport in Fe-limited *Thalassiosira weissflogii* from Anderson and Morel (1982), Harrison and Morel (1986) and Hudson and Morel (1990). For further details about the data for *T. weissflogii* see Hudson and Morel (1990). As indicated in the methods and legend of Table S3, *P. tricornutum* K_m for Cu (nM $[Cu]_{total}$ or pM [Cu′]) was calculated for $[Cu]_{total}$ (i.e., total Cu concentration in nM) and for [Cu′] (i.e., the dissolved inorganic Cu concentration in nM), which was calculated considering the presence of L_1 and L_2 released by the algae (Table 3).

	Kinetics parameters of Fe and Cu transport under low Me conditions			
	Fe*		Cu**	
	Thalassiosira weissflogii		*Phaeodactylum tricornutum*	
Surface area (μm²)	394		35	
Saturation kinetics			S_1	S_2
K_m (nM $[Fe]_{Total}$)	640	K_m (nM $[Cu]_T$)	154	2636
K_m (M Fe′)	3.1E−09	K_m (M Cu′)	8E−14	1.37E−12
V_{max} (amol cell^{-1} h^{-1})	180		0.0518	0.6755
V_{max} (amol μm^{-2} h^{-1})	0.456		0.00148	0.0193
Transporters				
Density (amol cell^{-1})	17–56		27.3	229.6
Density (× 10^{-18} mol μm^{-2})	0.043–0.142		0.78	6.56
k_f (M^{-1} s^{-1})	0.9–1.3 × 10^6	k_f (M^{-1} s^{-1})	1.10 × 10^7	3.01 × 10^5
k_d (s^{-1})	0–2 × 10^{-3}	k_d (s^{-1})	1.35 × 10^{-6}	4.50 × 10^{-3}
k_{in} (s^{-1})	0.9–3 × 10^{-3}	k_{in} (s^{-1})	5.27 × 10^{-7}	8.17 × 10^{-7}

* Hudson and Morel (1990).
** This study.

4.4. Cu-binding sites at the cell surface of *P. tricornutum* in the presence of low Cu concentrations

In this study, we measured the Cu-binding sites at the cell surface of *P. tricornutum* with adsorption isotherms, in the presence of 0–30 nM Cu concentrations. The Cu adsorption curve differs remarkably from previous studies (e.g., González-Dávila, 1995), exhibiting a biphasic shape. This result can be explained by the extremely low Cu concentrations added here, relative to those in previous studies (~10 nM–20 μM; Scarano and Morelli, 1999, González-Dávila et al., 2000). At our low Cu concentrations, an apparent competition between L_1 and S_1 for the added Cu exists and can be observed, unlike in previous studies with much higher Cu concentrations.

Our adsorption studies indicate that *P. tricornutum* cell surface presents low and high-affinity Cu-binging sites, with *log* K_{ads} ranging from 7.8 to 12.9 (Table 3). Furthermore, the density of these two types of Cu-binding cell surface sites differed by an order of magnitude, with an average surface density of $5.79 \cdot 10^{-18}$ and $6.68 \cdot 10^{-19}$ mol μm^{-2} for the low- and high-affinity sites, respectively (Table 3).

The low-affinity Cu-binding sites at the cell surface of *P. tricornutum* have a similar Cu^{2+} binding strength ($logK_{ads}^{Cu^{2+}} = 9.1–9.4$, Table 3) to those determined in previous adsorption studies using higher titration Cu additions (González-Dávila et al., 2000), and those for hydrous oxides of silicon (i.e., $logK_{ads}^{Cu^{2+}} = 9.6$; Motschi, 1984). Diatoms' cell wall is composed of amorphous, hydrated silicon dioxide (silica), that can bind proteins and polysaccharides (Kroger and Sumper, 1998). However, *P. tricornutum* cell wall, in contrast with other diatoms, is poor in silica (Le Costaouëc et al., 2017), which suggests that S_2 sites might have a physiological function, such as low-affinity Cu transport under high Cu concentrations. Indeed, after adding azide, only these S_2 sites remained detectable (Table 3), suggesting that reductive step is not involved in Cu transport via S_2 sites, as expected for non-specific divalent transporters, such as NRAMPs and ZIPs. In the case of *P. tricornutum*, we hypothesized that S_2 might be the putative ZIP transporter *Pt*ZIP49400 (Table 4).

Moreover, the density of the low- and high-affinity Cu-binding sites on the cell surface of *P. tricornutum* was significantly higher for the cells grown in the low Cu relative to the control (Table 3). In contrast, the affinity constants of the low- and high-affinity Cu-binding sites were not significantly different between the two growth treatments (Table 3). This indicates that *P. tricornutum* grown at different conditions exhibits Cu-binding sites with similar strengths. However, their density increases under low Cu availability, as previously observed for Fe uptake in diatoms (Harrison and Morel, 1986). Even though different Cu-binding sites may be present, and they exhibit a combined binding constant similar to the average one we determined.

4.5. Comparing high-affinity Cu-binding sites at the cell surface of *P. tricornutum* vs. high-affinity ligands released into solution by *P. tricornutum*

The high-affinity Cu-binding sites at the cell surface of *P. tricornutum* present similar affinity constants under the two growth conditions, with an average *log* K_{ads} of 12.9 ± 0.01 (Table 3). These high-affinity cell surface Cu-binding site constants are between L_1 and L_2 affinity constants for the ligands excreted by *P. tricornutum* in solution (Table 2).

Given that *P. tricornutum* can release strong organic complexes for Cu and take up Cu via high-affinity transport systems, these high-affinity ligands released in solution could compete for inorganic Cu with the transporters (i.e., high-affinity Cu transport system). To examine this possible interaction, the Cu-binding site concentrations were normalized to cell densities and expressed as mol L^{-1}. This normalization revealed that the concentration of the high-affinity Cu-binding sites on the cell surface ($1.6–1.8 \cdot 10^{-9}$ mol L^{-1}; Table 3) are an order of magnitude higher than the L_1 ligands released into solution by *P. tricornutum* ($2.9–3.8 \cdot 10^{-10}$ mol L^{-1}; Table 2). However, as indicated above, the Cu stability constant for L_1 is an order of magnitude higher than that of S_1, indicating that the excreted ligands are stronger than those at the cell surface. We combine both parameters to calculate the Cu complexing potential of S_1 and L_1, such that $f_{CuX_i} = [X_i'] \cdot K_{CuX_i}$, where X_i can be either L_i or S_i. The resulting log f_{CuX_i} for L_1 and S_1 are practically identical (4.16 ± 0.3 vs. 4.13 ± 0.2, Table 2), suggesting they have equal Cu complexing potential.

Under environmental Cu concentrations (0.1–1 nM Cu), in the presence of concentrations of L_1 and S_1 as found here (i.e., $L_1 + S_1 = 2$ nM), and assuming chemical equilibrium (i.e., ~10 min), over 99.99 % of the Cu will be organically complexed (Cu' from 0.0026 % to 0.0041 %), with the excreted L_1 ligands complexing 34 % to 20 %, L_2 between 3 % and 5 % while the surface ligand S_1 will bind 62 to 75 %, respectively. This calculation emphasizes the importance of the high-affinity cell surface ligands in the speciation of Cu in natural seawater, which has been previously ignored.

In surface waters where phytoplankton densities (e.g., coastal waters with $6 \cdot 10^3$ and $7 \cdot 10^4$ cell mL^{-1} for diatoms and coccolithophores as *Emiliania huxleyi*, respectively; (Segovia et al., 2017; Ruacho et al., 2022) may be as high as those in our cultures ($5–8 \cdot 10^4$ cells mL^{-1}), the Cu' would decrease from $0.1 \cdot 10^{-12}$ M (i.e., free Cu^{2+} concentration (pCu) $10^{-14.3}$) to $0.15 \cdot 10^{-15}$ M (i.e., pCu = $10^{-17.1}$), if phytoplankton are excreting L_1 and L_2 -like ligands and have cell surface binding ligands, as S_1 and S_2. The ligands excreted by *P. tricornutum* are in the high binding strength range (Ruacho et al., 2022). However, the free concentrations determined with both excreted and surface ligands, emphasizes the phytoplankton surface binding sites also play a key role in trace metal speciation in seawater.

However, the surface ocean is a highly dynamic system where chemical equilibrium is rarely achieved, and kinetic processes should be considered. In an attempt to examine kinetic processes affecting Cu complexation in surface waters, we calculated the forward and dissociation rate constants of Cu-binding ligands and cell surface sites of *P. tricornutum*. The forward and dissociation rate constants, with respect to Cu', were one order of magnitude faster for the Cu binding ligands released by *P. tricornutum* than for the high-affinity binding sites at its cell surface (i.e., S_1 vs. L_1 and L_2; Table 5). The Cu forward rate constants of S_1, relative to S_2, were two orders of magnitude faster, while the dissociation rate constants were three orders of magnitude slower. This confirms that S_1 has a higher affinity for Cu than S_2, as expected for a high-affinity Cu transporter.

To understand the implications of the relatively fast forward rate constant of S_1, which we assume is involved in high-affinity Cu transport, we must compare its k_f and k_d to the rate of Cu internalization by the cells (k_{in}, Hudson and Morel, 1993), which we measure using ^{64}Cu. This comparison will also allow us to determine whether Cu transport by phytoplankton in the surface waters is thermodynamically or kinetically controlled in the ocean.

4.6. Is the high-affinity Cu transport system in diatoms kinetically or thermodynamically controlled?

The *P. tricornutum* physiological and analytical chemistry data were combined to determine whether Cu uptake in marine phytoplankton is kinetically or thermodynamically controlled, as previously done for (Hudson and Morel, 1990, 1993; Hudson, 1998). A summary of these principles is introduced below.

The acquisition of essential cationic metals in phytoplankton may occur via transporter-facilitated uptake or extracellular chelator-mediated uptake, requiring the metal ion to undergo a series of ligand exchange reactions. Indeed, specific binding to the transporter is generally necessary for transporting essential transition metals (Eide, 1997). The paradigm of metal transporter-facilitated uptake kinetics in phytoplankton involves two steps: the reversible binding of the trace metal to the transporter, and irreversible transport into the cell. Indeed,

the plasma-membrane bound, transport sites for metal uptake behave as strong binding ligands at the cell surface. Under steady-state conditions, the rate of metal uptake follows typical Michaelis-Menten uptake kinetics, such as the maximum rate of uptake (ρ_{max}), and the half-saturation rate constant (K_m) are a direct function of the total number of metal transporters at the cell surface (S), the apparent kinetic rate constants for the complex formation (k_f), dissociation (k_d) and metal internalization (k_{in}) reactions. The kinetics of metal uptake by a membrane carrier can thus be thermodynamically or kinetically controlled (Fig. 3).

Often, it is assumed that the reaction between the transporters and the dissolved metal approaches equilibrium, so that the dissociation rate constant is much faster than the internalization step, resulting in a ratio of dissociation to forward rate constants of the metal transporter complex that is similar to that at equilibrium. In this thermodynamically controlled uptake system, the half-saturation constant for metal uptake (K_m) equals k_d/k_f. Thus, it is simply the inverse of the apparent metal-transporter ligand stability constant ($K'_{MS} = k_f/k_d$). In these thermodynamically-controlled uptake systems, the apparent metal-transporter binding is a function of the free metal ion activity or concentration. Thus, the half-saturation constant is often expressed as free metal concentration. Thermodynamically-controlled uptake systems are favored for metals whose speciation is dominated by inorganic complexes, and whose dissolved concentrations in the ocean are not growth-limiting. Furthermore, non-selective uptake systems, such as the Mn transporters studied by Sunda and Huntsman (1996), are thermodynamically-controlled. In this case, the uptake of one metal over the other (Mn, Zn vs. Cd) depends on the relative kinetics of each metal (fast kinetics favor equilibrium) and their affinity for the transporter site (weak binding favors equilibrium) (Hudson, 1998) (Fig. 3)

In contrast, kinetically-controlled uptake systems are observed when the internalization rate is faster than that of dissociation and results from the steady-state balance between the transport complex formation rate constant and the internalization rate constant. The half-saturation constant for metal uptake (K_m) equals the ratio of the two corresponding rate constants, k_{in}/k_f. These uptake rates depend on the total concentrations of inorganic metal species (i.e., M′). Thus, the half-saturation uptake kinetics are often expressed as M' concentrations (Fig. 3).

Hudson and Morel (1990) demonstrated that Fe uptake in two Fe-limited phytoplankton (*P. carterae* and *T. weissflogii*) was under kinetic control. In that study, Fe uptake was observed during a chase experiment, when the cells were not exposed to dissolved ^{55}Fe, suggesting that ^{55}Fe bound to the uptake sites was not in equilibrium with Fe species in solution, and thus uptake was kinetically controlled. However, no surface Fe uptake was observed for Fe-replete cells, suggesting that Fe uptake is thermodynamically controlled under Fe-replete conditions, or the number of transport sites is significantly lower, resulting in unmeasurable uptake rates.

In contrast, several studies and genomic data suggest *P. tricornutum* has three Fe acquisition mechanisms, which are kinetically or thermodynamically controlled (reviewed by Sutak et al., 2020). The first mechanism—non-reductive and thermodynamically controlled—acquires unchelated Fe species via endocytosis, after carbonate-dependent binding of Fe(III)′ to phytotransferrin ISIP2a at the cell surface (McQuaid et al., 2018). The second Fe acquisition mechanism is kinetically controlled and depends on the extracellular reduction of all iron species (Morrissey et al., 2015). The third Fe acquisition mechanism in *P. tricornutum* allows the transport of hydroxamate siderophores by endocytosis (dependent on ISIP1) after binding to the FBP1 protein, and iron is released from the siderophores by FRE2-dependent reduction (Kazamia et al., 2018).

In the *P. tricornutum* Cu uptake experiments, we identified a high- and low-affinity Cu transport system (Fig. 4). Similarly, the voltammetric determinations identified low- and high-affinity Cu-binding sites at the cell surface (S_2 and S_1) of *P. tricornutum*. Even though the high-affinity Cu transport system in *P. tricornutum* might include two components (i.e., Cu reductases followed by the high-affinity Cu^+ transporter CTR), the voltammetric measurements cannot distinguish the characteristics of these two components. However, our azide-voltammetric experiments may provide some clues. The azide results

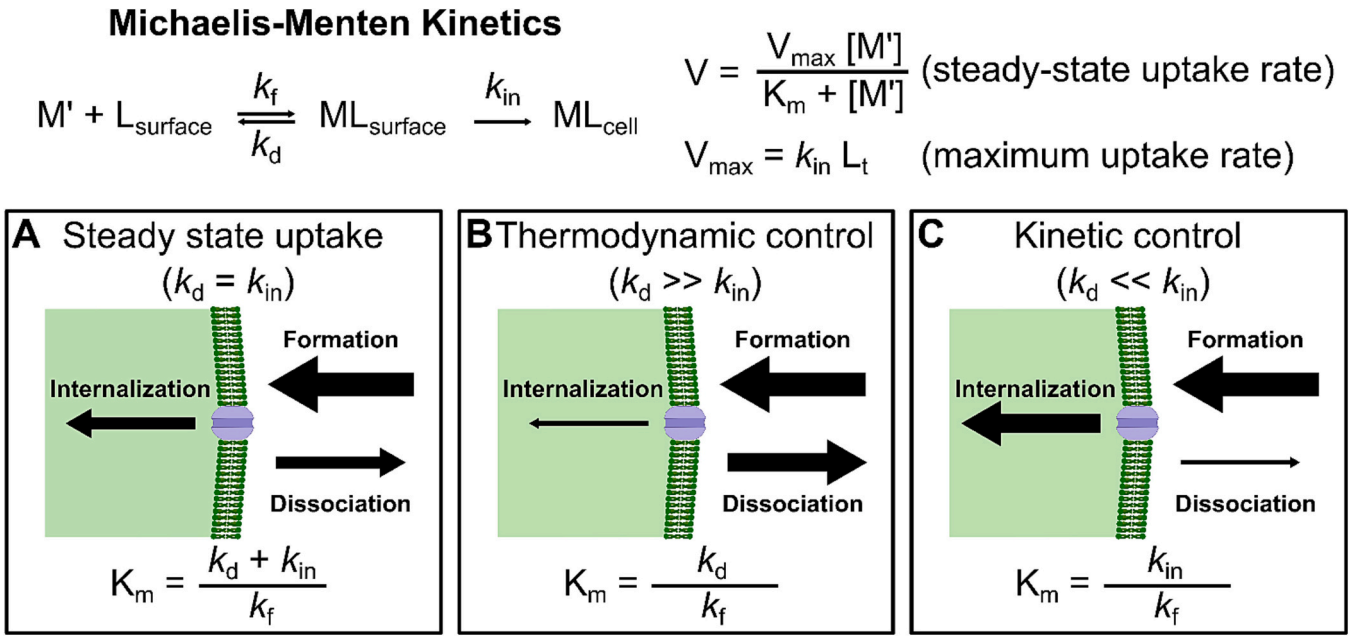

Fig. 3. Kinetics of metal uptake by membrane carriers, adapted from Fig. 1 in Hudson and Morel (1993). Michaelis-Menten parameters for steady-state transport (K_m and V_{max}) depend on the rate constants for metal-transport ligand ($ML_{surface}$) complex formation (k_f), dissociation (k_d) and internalization (k_{in}) and on the total number of transport ligands ($[L_t]$). Arrow widths indicate the relative rates of each reaction for undersaturated transport systems with the same number of total transport ligands. Since each system is assumed to have the same k_f the rate of complex formation is the same in all cases. (A) Steady-state transport, where the rate constants of dissociation (k_d) and internalization (k_{in}) are approximately the same. (B) Thermodynamically-controlled transport, where $k_d \gg k_{in}$. (C) Kinetically-controlled transport, where $k_{in} \gg k_d$.

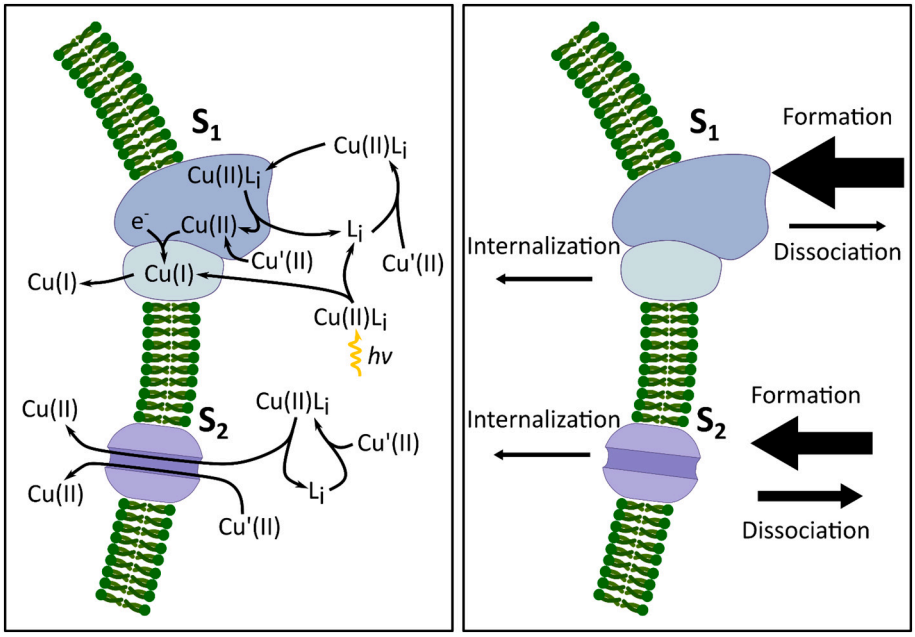

Fig. 4. Proposed conceptual model of Cu uptake by *P. tricornutum* based on our results. (A) Putative components of the high-affinity (S_1) and low-affinity Cu transport (S_2) systems (i.e., Cu-binding sites at the cell surface), and possible Cu species involved in the process. For S_1, Cu(II)′ represents inorganic Cu(II) species; L_i represents the strong organic Cu ligands (i.e., L_1 and L_2) excreted by *P. tricornutum*. Both, Cu(II)′ and organically complexed Cu(II)L_i are reduced to Cu(I) by a membrane-bound reductase or a light-mediated process, before internalization of Cu(I) by CTR-FRE complex, as previously shown (ref.). For S_2, Cu(II) is internalized without a reductive step. (B) The relative rate constants—formation (k_f), dissociation (k_d) and internalization (k_{in})—for the high- and low-affinity Cu-binding sites (i.e., S_1 and S_2, respectively), combining kinetic Cu uptake data with Cu adsorption and complexation parameters. Arrow widths indicate the relative rates of each reaction for S_1 versus S_2, accounting for differences in the number of transport ligands.

indicate that the S_2 Cu-binding sites, which remained active after the azide addition, are likely low-affinity Cu^{2+} transporters, with no reductase activity. In contrast, S_1 Cu-binding sites seem to be involved in high-affinity Cu transport, which likely includes the reduction of Cu^{2+} to Cu^{+}, and the internalization of Cu^{+}, given that azide—an electron transfer inhibitor—demolished its activity.

Interestingly, one of the putative high-affinity Cu transporters of *P. tricornutum* identified here, *Pt*CTR49224, and one identified in *T. oceanica* 1005 (i.e., *To*CTR3a: EJK74005; Kong and Price, 2019) have the conserved motifs of the N-terminus of the CTR1 protein in *H. sapiens* (*h*CTR1: AAB66306), which does not have a complementary reductase, but instead the Cu^{2+} reduction occurs within the *h*CTR1 or abiotically

(a)

```
PtCTR     ------------------------------------MDMGMAT   7
ToCTR3a   MCVSNMPMNTGTSPSGMNATSPMSSAGSMPAPAPTGPMGMGT  42
hCTR1     --------------------------------MDHSHHMGMSY  11
                                                ***.
PtCTR     --AAD-----------SFCTSSMGGG--MIMYMDGFRFSLKG  34
ToCTR3a   MDTAP---PPAGGPVPM--TMPAGSPMPHMGSMHGYFF----  75
hCTR1     MDSNSTMQPSHHHPTTSASHSHGGGDSSMMMMPMTFYF----  49
            :                        *.   :     : *
PtCTR     GQPCLNLFFPEWTLDSKGKF  54
ToCTR3a   GGPGFYYLFGGWFVSTTPQ-  94
hCTR1     GFKNVELLFSGLVINTAGE-  68
          *  .   :*    :.:  :
```

(b)

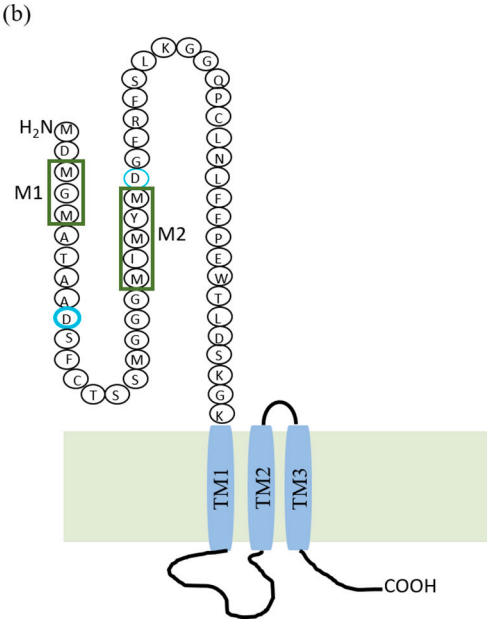

Fig. 5. Conserved motifs of the N-terminus of CTR proteins of *P. tricornutum* (*Pt*CTR49224: EEC44514), *T. oceanica* CCMP1005 (*To*CTR3a: EJK74005) and *H. sapiens* (*h*CTR1: AAB66306). (a) Amino acid sequences of the conserved motif in N-terminus of CTRs aligned using Clustal Omega (http://www.ebi.ac.uk/Tools/msa/clustalo/; Sievers et al., 2011). Asterisks, colons and periods represent identical, strongly similar and weakly similar residues, respectively. (b) Illustration of the *Pt*CTR N-term methionine (green rectangles) and aspartic (blue circles) acid residues which might be critical for copper import.

outside the cell (Kar et al., 2022; Janoš et al., 2022) (Fig. 5).

Just like the *h*CTR1 (Kar et al., 2022), *P. tricornutum* and *T. oceanica* 1005 have the M1 and M2 motifs—composed of a series of methionines—as well as the aspartate residue (D10 in blue color, Fig. 5) which corresponds to the residue D13 motif in *h*CTR1 (Kar et al., 2022). In addition, *P. tricornutum* has the D26 residue next to the M2 motif (Fig. 5) which is similar to the D37 motif of *h*CTR1 (Kar et al., 2022), but this motif is lacking in *To*CTR3a. But, in contrast to *h*CTR1, *Pt*CTR49224 and *To*CTR3a lack histidines in the N-terminal (Fig. 5).

Methionine clusters, in combination with aspartates on the *h*CTR1 N-terminal domain, facilitate reduction, binding, and stabilization of the reduced Cu^{+}. Eventually, the Cu^{+} enters the pore via its interaction with methionine triads, situated on the entrance of the Cu transporting pore (Kar et al., 2022). M1 serves as the first coordinator for Cu^{+}. The histidine motifs in *h*CTR1 (i.e., H1 and H2 in *h*CTR1)—which are lacking in the CTR of *To*CTR3a and *Pt*CTR49224—are not essential, but increase the Cu^{2+} concentrations at the vicinity of *h*CTR1 under Cu-limiting conditions, for further reduction and uptake.

The D13 motif in *h*CTR1 is indispensable for Cu^{2+} binding, and plays a crucial role in transiently binding and shuttling Cu^{+} to either M1 or M2 (Kar et al., 2022). M1 motif in *h*CTR1 is key for Cu^{+} uptake, but can be functionally complemented by M2. When

*h*CTR1 is provided with a source of Cu^{2+}, the protein in combination with other external reducing agents, reduces Cu^{2+} to Cu^{+}. But, either M1 or M2 need to be present for Cu^{+} transport into the cell. The motif D13 (i.e., an aspartate residue) is also required for Cu^{+} to be internalized, and aspartate might act as a transient binder for Cu^{2+} and Cu^{+} during the reduction process and thereby facilitate shuttling of the ion from its Cu^{2+} state to the adjacent methionine Cu^{+} state. Indeed, *h*CTR1 can reduce Cu^{2+} to Cu^{+}, which is facilitated by the second methionine stretch, M2. Whether M2 participates in the Cu^{2+} reduction or not, it depends on its extracellular solvent accessibility. Thus, given the similarity between *H. sapiens h*CTR1and *P. tricornutum Pt*CTR49224, it is also possible that the high-affinity Cu transporter in *P. tricornutum* has the ability to also reduce Cu^{2+} to Cu^{+}, before internalization.

The high-affinity Cu binding sites at the cell surface of *P. tricornutum* (S_1) should correspond with a Cu-specific, high-affinity Cu transporter, whose activity is enhanced under low Cu (Fig. 4). In support of this, we found a significantly higher density of high-affinity Cu binding sites (mol μm^{-2}) at the cell surface of *P. tricornutum* when grown in low Cu relative to the control. Our results also show identical binding strength for Cu by these high-affinity Cu binding sites at the surface of cells acclimated to both growth media. Methionine (M) forms with Cu^{2+} a CuM_2 complex using two donors with formation constant of log K 14.52 ± 0.01 in different aqueous media (see Table 4.4 in Berthon, 1995). Moreover, a Cu^{+} Chloride Methionine mixed-ligand complex $Cu^{+}ClM$, with complexation constant of 14.49 was reported (see Table 4.6 in Berthon, 1995). These values are similar to that determined in our study (Table 3), even when our voltammetry method provides an average value for any high affinity binding site and cannot distinguish between Cu(II) and Cu(I). *P. tricornutum* does not seem to introduce additional Cu-binding specific functional groups that modify the complexing strength of the high-affinity Cu binding sites used in control conditions. However, it is also possible that new ligands were activated on the cell surface but had the same binding strength as those in the control conditions and/or had complexing properties outside our experimental detection window (Campos and van den Berg, 1994).

Combining our voltammetric results for the dissociation and formation rate constants (Table 5), as well as the density (Table 3) of the Cu-binding sites (S_1 and S_2) at the cell surface of *P. tricornutum*, with the Cu uptake kinetics parameters of the high- and low- affinity Cu transport systems in *P. tricornutum* (Table 1 and S3) we were able to compare a series of Cu transport parameters (Tables 6 and S3).

For example, given that the maximum rate of Cu uptake is a function of the density of Cu transporters (i.e., $[S_1]$ and $[S_2]$) and the internalization rate constant for Cu (k_{in}^{S1} and k_{in}^{S2}) such that $V_{max} = [S_1] * k_{in}$, we solved for k_{in} of the high- and low-affinity Cu transport system for *P. tricornutum*. The calculated internalization rate constants for Cu uptake are $5.27 \cdot 10^{-7}\ s^{-1}$ for k_{in}^{S1} and $8.17 \cdot 10^{-7}\ s^{-1}$ for k_{in}^{S2} (Table 6).

Moreover, kinetically-controlled uptake systems are observed when the internalization rate is faster than that of dissociation. In the case of the high-affinity Cu transporter, S_1, the rates of internalization for *P. tricornutum* ($5.27 \cdot 10^{-7}\ s^{-1}$) are very similar to those of dissociation of Cu′ from S_1 ($1.3 \cdot 10^{-6}\ s^{-1}$, Table 3), suggesting that high-affinity Cu uptake is borderline between being a kinetically or thermodynamically controlled. In contrast, for the low-affinity Cu transporters, S_2, the Cu′ dissociation rate constant ($5.9 \cdot 10^{-3}\ s^{-1}$) is 4 orders of magnitude faster than that for its internalization ($8.17 \cdot 10^{-7}\ s^{-1}$), implying an explicit thermodynamic control (Fig. 4).

4.7. Comparing the kinetic parameters of Fe and Cu uptake by *T. weissflogii* and *P. tricornutum* grown in low metal conditions

Given the link between Fe and Cu nutrition in marine diatoms (Peers et al., 2005; Maldonado et al., 2006; Annett et al., 2008; Guo et al., 2010, 2015), and the interest and knowledge on Fe transport and homeostasis, here we compared the findings of Hudson and Morel, 1990, 1993) on Fe uptake kinetics in the model diatom *T. weissflogii* and our new findings on Cu uptake kinetics in *P. tricornutum* (Tables 6, S3). We focused on the transport systems observed under low metal conditions for these comparisons and normalized all the pertinent cellular parameters to cell surface area.

The density of the cell surface S_1 Cu transporters (0.78 amol μm^{-2}) is an order of magnitude higher than that for Fe (0.043–0.142 amol μm^{-2}). The half-saturation constants for Fe and Cu uptake in Fe- and Cu-stressed diatoms, respectively, expressed as total Fe and Cu concentrations, did not differ greatly (i.e., by 4-fold) but was slightly lower for Cu (154 nM Cu) than for Fe uptake (640 nM Fe) (Table 6), though given the errors of these estimates (e.g., Table 1), these half-saturation constants are practically identical.

However, when these half-saturation constants are expressed as inorganic Cu or Fe concentrations, the K_m differed by five orders of magnitude and was significantly lower for Cu (i.e., 0.08 pM Cu′ vs. 3.1 nM Fe′). Given the direct relationship between the values of K_m and V_{max}, as expected, the V_{max} of Cu uptake (0.00148 amol $\mu m^{-2}\ h^{-1}$) is significantly lower (by ~300-fold) than that of Fe (0.456 amol $\mu m^{-2}\ h^{-1}$, Table 6). The differences in Fe and Cu uptake kinetics can be explained by the kinetics of their respective transporters. While the forward rate constants of the putative Cu and Fe transporters are within an order of magnitude from each other (i.e., $1.1 \cdot 10^{7}\ M^{-1}\ s^{-1}$ and $0.9–1.3 \cdot 10^{6}\ M^{-1}\ s^{-1}$, respectively), the rate constants of dissociation ($1.35 \cdot 10^{-6}\ s^{-1}$ and $0–2 \cdot 10^{-3}\ s^{-1}$, respectively) and 'calculated' internalization ($5.27 \cdot 10^{-7}\ s^{-1}$ and $0.9–3 \cdot 10^{-3}\ s^{-1}$ respectively) are 34 orders of magnitude slower for Cu than Fe (Table 6). Moreover, the slow internalization kinetics for Cu are due to the strong thermodynamic stability of the CuS_1 complex. This results in a large quantity of Cu bound to the transport sites relative to the Cu internalized into the cell. Compared to Fe, the relatively high concentrations of Cu in seawater, imply that Cu can be easily internalized, possibly resulting in detrimental toxic effects for phytoplankton, unless strictly regulated at the transport sites. The high affinity and low velocity of the Cu-transporters will ensure that Cu uptake is carefully controlled. Indeed, the internalization of Cu is tightly regulated by the CTR1 transporter via two methionine triads, which form a selectivity filter, enabling selective Cu^{+} transport and regulating its uptake rate (Janoš et al., 2022).

4.8. Comparisons of measured vs. calculated formation rate constant of metal-transporter complex (k_f) at the cell surface of diatoms

Hudson and Morel (1993) discussed that their derived forward rate constant (k_f) for inorganic Fe uptake ($0.9–1.3 \times 10^{6}\ M^{-1}\ s^{-1}$) was much faster than the water loss kinetic constant of Fe^{3+} and $FeOH^{2+}$ (Monzyk

and Crumbliss, 1982), but within a factor of 2 of the conditional rate constant for Fe complexation by the siderophore Desferal B (2×10^6 M^{-1} s^{-1}, Hudson et al., 1992). They suggested that Fe-limited phytoplankton maximize the coordination kinetics of Fe transport, and that the kinetics of metal binding to the transporter is near rates limited by water exchange kinetics for $Fe(OH)_2^+$ and $Fe(OH)_4^-$. As Hudson and Morel (1993) discussed, a kinetically-controlled uptake system would be favored for trace metals with slow water exchange kinetics and low environmental concentrations.

The forward rate constant (i.e., k_f of $1.1 \cdot 10^7$ M^{-1} s^{-1}) we determined for the high-affinity Cu transport sites (S_1) at the cell surface of *P. tricornutum* are 2-orders of magnitude slower than the ones calculated for Cu ($1 \cdot 10^9$ M^{-1} s^{-1}) by Hudson and Morel (1993)—see Table 1 (Hudson and Morel, 1993)—based on the product of the outer-sphere complex stability (K_{OS}) and the rate of water loss (k_{-w}) so that $k_f = K_{OS} \cdot k_{-w}$. If we assume a complex formation rate constant of 10^9 M^{-1} s^{-1}, as suggested by Hudson and Morel (1993), given the Cu binding constant for S_1 we measured ($log K_{ads_1}$) of ~13 (Table 3), the dissociation rate constant would be in the order of $1 \cdot 10^{-4}$ s^{-1}. These formation and dissociation constants will result in Cu adsorption onto the cell surface, reaching equilibrium within a few seconds, far from the 10 min we, and others, measured (González-Dávila, 1995 and references herein). Our measurements suggest that, at least for Cu, the phytoplankton do not maximize the coordination kinetics of Cu transport. Thus, extrapolating a forward rate constant for Cu—based on the product of the outer-sphere complex stability (K_{OS}) and the rate of water loss (k_{-w})—in solution to that of the Cu-binding cell surface sites is inappropriate.

Based on their calculations of the minimum number of transport ligands at the cell surface of *T. weissflogii*—needed to fulfill cellular metal requirements—they argued that for Ni, Zn and Fe, due to slow reaction kinetics and low concentrations in surface waters, the concentration of free transport ligands at the cell surface ($[L']_{min}$) has to be similar to the cellular metal concentration ($Q_{0.9}$) and that this poses serious challenges for the phytoplankton.

Hudson and Morel (1993) did not calculate $[L']_{min}$ for Cu because diatoms' Cu requirements were unknown (Table S4). Data on Cu requirements of oceanic diatoms (Annett et al., 2008) allowed us to calculate the minimum number of transport ligands at the cell surface of *T. weissflogii* needed to fulfill cellular demand. Using the forward rate constant, we measured for S_1 (k_f of $1.1 \cdot 10^7$ M^{-1} s^{-1}), the $[L']_{min}$ at the cell surface of *P. tricornutum* is estimated to be relatively high (4 amol $cell^{-1}$) compared to a Cu demand of 2 amol $cell^{-1}$ (Table S4). Our measured S_1 density at the cell surface is significantly higher than this minimum number of Cu transport ligands, which suggests that *P. tricornutum* must control Cu uptake, as indicated above.

4.9. Metal concentrations in the surface ocean

As suggested by Redfield in 1958 (Redfield, 1958), the chemical stoichiometry of phytoplankton and seawater are well linked. We might then ask, what determines how low phytoplankton can deplete trace metal concentrations in the surface ocean? While exploring this question, Hudson and Morel (1993) highlighted a significant negative correlation between essential inorganic trace metals' concentrations in oceanic surface waters and the formation rate constants (k_f) of the respective trace metal transport sites at the phytoplankton cell surface. They suggested that this very significant relationship might indicate that kinetic lability controls the bioavailability of these essential metals and their removal rate from surface waters. Surprisingly, while the relationship was excellent for Fe, Ni, Zn, Co and Cd, it was poor for Cu and Mn. An unrealistically high value of k_f for Cu was suggested to explain the Cu deviation. Using our measured S_1 k_f for Cu, the relationship between the concentrations of essential inorganic trace metals in oceanic surface waters and the forward rate constants (k_f) for the trace metal transporter sites is greatly improved (excluding Mn, r^2 of the regressions are 0.92 vs. 0.90), and the slope is almost unity (−0.99 vs −0.8) (Fig. 6, Table S4).

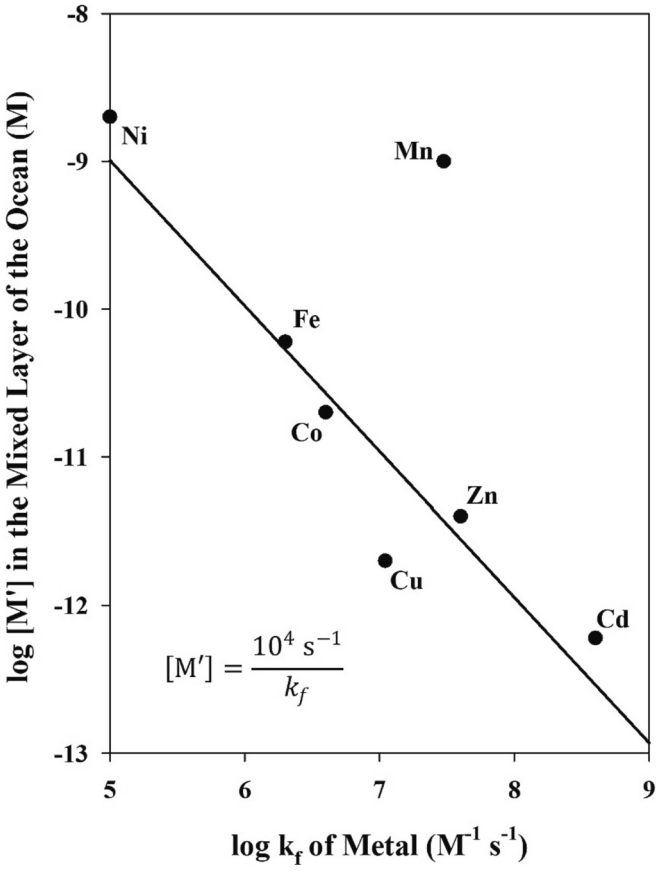

Fig. 6. Correlation between the concentrations of inorganic bioactive metals [M′] in surface waters and the formation rate constants (k_f) of the metal to the transport sites at the cell surface of phytoplankton. The k_f for Fe and Cu were measured in Hudson et al. (1992), and in this study (Table 4), respectively. For the remaining metals, k_f were calculated by Hudson and Morel (1993) based on the product of the outer-sphere complex stability (K_{OS}) and the rate of water loss (k_{-w}) (see main text). All data are from Table S3. Regression line exclude the Mn data ($r^2 = 0.92$, slope = −0.99).

5. Conclusions

The combination of the fields of 'omics, physiology and physical chemistry provides a unique understanding of the close link and interaction between seawater and phytoplankton. Fe and Cu are essential trace metals for phytoplankton, and their physiologies are closely linked. But Fe is the most important trace metal for phytoplankton growth, resulting in cellular Fe stoichiometries 10 times higher than those of Cu (reviewed by Twining and Baines, 2013). In the ocean, the speciation of dissolved Fe and Cu are similarly dominated by strong organic ligands complexation. But, while concentrations of dissolved Fe in surface waters are in the picomolar range (~0.07 nM, Johnson et al., 1997), those of Cu are in the nanomolar range (0.1 to 5 nM, Cui and Gnanadesikan, 2022). The contrasting phytoplankton requirements for Fe and Cu, and the Fe and Cu concentrations in the ocean begs the question of whether Fe and Cu transport systems in phytoplankton are differentially controlled.

To answer this question, we performed physiological and physicochemical experiments using the model diatom, *Phaeodactylum tricornutum*, grown in natural North Atlantic seawater. First, using competitive ligand equilibration-cathodic stripping voltammetry (CLE-CSV), we measured the concentrations and stability constants for Cu of organic ligands released by *P. tricornutum*, and showed that the cells released

two strong soluble Cu-binding ligand types (L_1 and L_2), with concentrations of L_2 ligands one order of magnitude higher than those of L_1 (i.e., ~0.35 nM L_1 and 1.3 nM L_2). The function of this ligands is unknown but given that the Cu concentrations were non-toxic (i.e., 0.44 nM), it is possible that these ligands are released to enhance Cu uptake.

We also established the density and stability constants of two putative Cu transporters at the cell surface of *P. tricornutum* (i.e., low- and high-affinity, S_2 and S_1, respectively)—as well as the rate constants for complexation, dissociation. Their log *K* differed by 5 orders of magnitude, while their cell surface densities varied by 9-fold.

Using complementary Cu uptake experiments, we identified a high- and a low-affinity Cu uptake system in *P. tricornutum*, which nicely agreed with the voltammetric determinations that identified low- and high-affinity Cu-binding sites at the cell surface (S_2 and S_1) of *P. tricornutum*. The azide experiments suggest that S_2 Cu-binding sites are likely low-affinity Cu^{2+} transporters, with no reductase activity. In contrast, S_1 Cu-binding sites seem to be involved in high-affinity Cu transport, which likely include a reduction step from Cu^{2+} to Cu^{+}, before Cu^{+} is internalized. We examined the published *P. tricornutum* genome for potential genes encoding high- and low-affinity Cu transporters. We identified *Pt*CTR49224, as the high-affinity Cu^{+} transporter, given its high homology to other identified high-affinity Cu^{+} transporters: *T. oceanica To*CTR3a and *Homo sapiens h*CTR1. Interestingly, *h*CTR1 does not have a complementary reductase, but instead the Cu^{2+} reduction occurs within the *h*CTR1 or abiotically outside the cell, depending on the accessibility to extracellular reducing agents. So, whether *Pt*CTR49224 itself is involved in the reduction of Cu^{2+} to Cu^{+} before internalization, or reduction of Cu^{2+} occurs extracellularly either abiotically or biotically (i.e., via cell surface reductase) remains to be determined.

We identified five putative ZIP-like transporters in *P. tricornutum*, but highlighted *Pt*ZIP49400 as the low-affinity Cu transporter identified with voltammetry (S_2), given that *Pt*ZIP49400 is a homolog to *T. pseudonana Tp*ZIP268980, which was downregulated in Cu-limited *T. pseudonana* cultures.

Voltammetric kinetic measurements and a theoretical kinetic model allowed us to calculate the forward and dissociation rate constants of L_1 and L_2, as well as and S_1 and S_2. These physiological and physicochemical data were combined to calculate the rate constant for the internalization of Cu in *P. tricornutum*. We established that while high-affinity Cu uptake system (S_1) is borderline between a kinetically or thermodynamically controlled system, the low-affinity Cu transporters, S_2, is thermodynamically-controlled. We compared the kinetics of high-affinity Cu uptake (in *P. tricornutum*) and Fe uptake (in *T. weissflogii*) and concluded that they were explained by the kinetics of their respective transporters. While the forward rate constants of the putative Cu and Fe transporters are within an order of magnitude from each other, the rate constants and 'calculated' internalization were 34 orders of magnitude slower for Cu than Fe. Moreover, the slow internalization kinetics for Cu are due to the strong thermodynamic stability of the CuS_1 complex. This results in a large quantity of Cu bound to the transport sites relative to the Cu internalized into the cell. Compared to Fe, the relatively high concentrations of Cu in seawater, imply that Cu can be easily internalized, possibly resulting in detrimental toxic effects for phytoplankton, unless strictly regulated at the transport sites. The high affinity and low velocity of the Cu-transporters will ensure that Cu uptake is carefully controlled.

We revised the inverse relationship between the surface ocean concentrations of inorganic complexes of the essential metals (i.e., Ni, Fe, Co, Zn, Cd, Mn and Cu) and the formation rate constant of metal transporters at the cell surface of phytoplankton, highlighting the link between the chemical properties of phytoplankton metal transporters and the availability and speciation of trace metals in the surface ocean. The rate constants we determined for Cu formation, dissociation and internalization by surface and excreted ligands will be helpful for modelers interested in the biogeochemical cycling of Cu in the ocean.

CRediT authorship contribution statement

Melchor González-Dávila: Conceptualization, Formal analysis, Funding acquisition, Investigation, Methodology, Validation, Writing – original draft, Writing – review & editing, Data curation, Resources, Supervision. **Maria T. Maldonado:** Conceptualization, Formal analysis, Investigation, Methodology, Supervision, Validation, Writing – original draft, Writing – review & editing. **Aridane G. González:** Conceptualization, Data curation, Formal analysis, Investigation, Methodology, Validation, Writing – original draft, Writing – review & editing. **Jian Guo:** Data curation, Formal analysis, Methodology, Supervision, Writing – original draft, Writing – review & editing. **David González-Santana:** Conceptualization, Data curation, Formal analysis, Methodology, Software, Supervision, Writing – original draft, Writing – review & editing. **Antera Martel:** Methodology, Resources, Visualization, Writing – original draft. **J. Magdalena Santana-Casiano:** Conceptualization, Data curation, Formal analysis, Funding acquisition, Investigation, Methodology, Supervision, Validation, Writing – original draft, Writing – review & editing.

Declaration of competing interest

The authors declare that they have no financial or non-financial interests to disclose. No conflicts are applicable to this study.

Data availability

Data will be made available on request.

Acknowledgements

This study received financial support from the FeRIA project (PID2021-123997NB-100) by the Spanish Ministerio de Ciencia e Innovación. It was also partially funded by the Natural Sciences and Engineering Research Council of Canada under grant RGPIN-2018-04827, and by the TRIUMF Life Science Program. We especially thank Prof. Paul Schaffer for providing Cu-64 for the uptake experiments.

Appendix A. Supplementary data

Supplementary data to this article can be found online at https://doi.org/10.1016/j.scitotenv.2024.170752.

References

Ajeesh Krishna, T.P., Maharajan, T., Victor Roch, G., Ignacimuthu, S., Antony Ceasar, S., 2020. Structure, function, regulation and phylogenetic relationship of ZIP family transporters of plants. Front. Plant Sci. 11 https://doi.org/10.3389/fpls.2020.00662.

Allen, A.E., LaRoche, J., Maheswari, U., Lommer, M., Schauer, N., Lopez, P.J., et al., 2008. Whole-cell response of the pennate diatom *Phaeodactylum tricornutum* to iron starvation. Proc. Natl. Acad. Sci. 105, 10438–10443.

Anderson, M.A., Morel, F.M.M., 1982. The influence of aqueous iron chemistry on the uptake of iron by the coastal diatom *Thalassiosira weissflogii*. Limnol. Oceanogr. 27, 789–813. https://doi.org/10.4319/lo.1982.27.5.0789.

Annett, A.L., Lapi, S., Ruth, T.J., Maldonado, M.T., 2008. The effects of Cu and Fe availability on the growth and Cu:C ratios of marine diatoms. Limnol. Oceanogr. 53 (6), 2451–2461.

Askwith, C., Eide, D., Van Ho, A., Bernard, P.S., Li, L., Davis-Kaplan, S., et al., 1994. The FET3 gene of *S. cerevisiae* encodes a multicopper oxidase required for ferrous iron uptake. Cell 76, 403–410. https://doi.org/10.1016/0092-8674(94)90346-8.

Barałkiewicz, D., Chudzińska, M., Szpakowska, B., Świerk, D., Gołdyn, R., Dondajewska, R., 2014. Storm water contamination and its effect on the quality of urban surface waters. Environ. Monit. Assess. 186, 6789–6803. https://doi.org/10.1007/s10661-014-3889-0.

Barber, R.T., Ryther, J.H., 1969. Organic chelators: factors affecting primary production in the Cromwell current upwelling. J. Exp. Mar. Biol. Ecol. 3, 191–199. https://doi.org/10.1016/0022-0981(69)90017-3.

Bartual, A., Gálvez, J.A., Ojeda, F., 2008. Phenotypic response of the diatom *Phaeodactylum tricornutum* Bohlin to experimental changes in the inorganic carbon system. Bot. Mar. 51, 350–359. https://doi.org/10.1515/BOT.2008.047.

van den Berg, C.M.G., Merks, A.G.A., Duursma, E.K., 1987. Organic complexation and its control of the dissolved concentrations of copper and zinc in the Scheldt estuary.

Estuar. Coast. Shelf Sci. 24, 785–797. https://doi.org/10.1016/0272-7714(87)90152-1.
Berthon, G., 1995. The stability constants of metal complexes of amino acids with polar side chains. Pure Appl. Chem. 67 (7), 1117–1240. https://doi.org/10.1351/pac199567071117.
Beveridge, T.J., Murray, R.G., 1980. Sites of metal deposition in the cell wall of *Bacillus subtilis*. J. Bacteriol. 141, 876–887. https://doi.org/10.1128/jb.141.2.876-887.1980.
Brand, L.E., 1985. Low genetic variability in reproduction rates in populations of *Prorocentrum micans* Ehrenb. (Dinophyceae) over Georges Bank. J. Exp. Mar. Biol. Ecol. 88, 55–65.
Buck, K.N., Ross, J.R.M., Russell Flegal, A., Bruland, K.W., 2007. A review of total dissolved copper and its chemical speciation in San Francisco Bay, California. Environ. Res. 105, 5–19. https://doi.org/10.1016/j.envres.2006.07.006.
Buck, K.N., Selph, K.E., Barbeau, K.A., 2010. Iron-binding ligand production and copper speciation in an incubation experiment of Antarctic Peninsula shelf waters from the Bransfield Strait, Southern Ocean. Mar. Chem. 122, 148–159. https://doi.org/10.1016/j.marchem.2010.06.002.
Campos, M.L.A.M., van den Berg, C.M., 1994. Determination of copper complexation in sea water by cathodic stripping voltammetry and ligand competition with salicylaldoxime. Anal. Chim. Acta 284, 481–496. https://doi.org/10.1016/0003-2670(94)85055-0.
Carić, H., Cukrov, N., Omanović, D., 2021. Nautical tourism in marine protected areas (MPAs): evaluating an impact of copper emission from antifouling coating. Sustainability (Switzerland) 13, 11897. https://doi.org/10.3390/su132111897.
Chadd, H.E., Newman, J., Mann, N.H., Carr, N.G., 1996. Identification of iron superoxide dismutase and a copper/zinc superoxide dismutase enzyme activity within the marine cyanobacterium *Synechococcus* sp. WH 7803. Microbiol. Lett. 138, 161–165. https://doi.org/10.1111/j.1574-6968.1996.tb08150.x.
Chretien, A.R.N., 1997. Geochemical Behaviour, Fate and Impacts of Cu, Cd and Zn from Mine Effluent Discharges in Howe Sound. Thesis.. University of British Columbia. https://doi.org/10.14288/1.0053151.
Coale, K.H., Bruland, K.W., 1988. Copper complexation in the Northeast Pacific. Limnol. Oceanogr. 33, 1084–1101. https://doi.org/10.4319/lo.1988.33.5.1084.
Coale, K.H., Bruland, K.W., 1990. Spatial and temporal variability in copper complexation in the North Pacific. Deep Sea Res. A Oceanogr. Res. Pap. 37, 317–336. https://doi.org/10.1016/0198-0149(90)90130-N.
Croot, P.L., Moffett, J.W., Luther, G.W., 1999. Polarographic determination of half-wave potentials for copper-organic complexes in seawater. Mar. Chem. 67, 219–232. https://doi.org/10.1016/S0304-4203(99)00054-7.
Croot, P.L., Moffett, J.W., Brand, L.E., 2000. Production of extracellular Cu complexing ligands by eucaryotic phytoplankton in response to Cu stress. Limnol. Oceanogr. 45, 619–627. https://doi.org/10.4319/lo.2000.45.3.0619.
Cui, M., Gnanadesikan, A., 2022. Characterizing the roles of biogeochemical cycling and ocean circulation in regulating marine copper distributions. J. Geophys. Res. Oceans 127. https://doi.org/10.1029/2021JC017742.
Dancis, A., Yuan, D.S., Haile, D., Askwith, C., Eide, D., Moehle, C., Kaplan, J., Klausner, R.D., 1994. Molecular characterization of a copper transport protein in *S. cerevisiae*: an unexpected role for copper in iron transport. Cell 2, 393–402. https://doi.org/10.1016/0092-8674(94)90345-X.
Dupont, C.L., Nelson, R.K., Bashir, S., Moffett, J.W., Ahner, B.A., 2004. Novel copper-binding and nitrogen-rich thiols produced and exuded by *Emiliania huxleyi*. Limnol. Oceanogr. 49, 1754–1762. https://doi.org/10.4319/lo.2004.49.5.1754.
Echeveste, P., Croot, P., von Dassow, P., 2018. Differences in the sensitivity to Cu and ligand production of coastal vs offshore strains of *Emiliania huxleyi*. Sci. Total Environ. 625, 1673–1680. https://doi.org/10.1016/j.scitotenv.2017.10.050.
Eide, D., 1997. Molecular biology of iron and zinc uptake in eukaryotes. Curr. Opin. Cell Biol. 9, 573–577. Available at: https://Ilbiomednet.com/elecref/095506740090057 3.
Fein, J.B., Daughney, C.J., Yee, N., Davis, T.A., 1997. A chemical equilibrium model for metal adsorption onto bacterial surfaces. Geochim. Cosmochim. Acta 61, 3319–3328.
González, A.G., Shirokova, L.S., Pokrovsky, O.S., Emnova, E.E., Martínez, R.E., Santana-Casiano, J.M., et al., 2010. Adsorption of copper on *Pseudomonas aureofaciens*: protective role of surface exopolysaccharides. J. Colloid Interface Sci. 350, 305–314. https://doi.org/10.1016/j.jcis.2010.06.020.
González-Dávila, M., 1995. The role of phytoplankton cells on the control of heavy metal concentration in seawater. Mar. Chem. 48, 215–236. https://doi.org/10.1016/0304-4203(94)00045-F.
Gonzalez-Davila, M., Santana-Casiano, J.M., Perez-Pena, J., Millero, F.J., 1995. Binding of Cu(II) to the surface and exudates of the alga *Dunaliella tertiolecta* in seawater. Environ. Sci. Technol. 29, 289–301. https://doi.org/10.1021/es00002a004.
González-Dávila, M., Santana-Casiano, J.M., Laglera, L.M., 2000. Copper adsorption in diatom cultures. Mar. Chem. 70, 161–170. https://doi.org/10.1016/S0304-4203(00)00020-7.
González-Santana, D., Planquette, H., Cheize, M., Whitby, H., Gourain, A., Holmes, T., et al., 2020. Processes driving iron and manganese dispersal from the TAG hydrothermal plume (mid-Atlantic ridge): results from a GEOTRACES process study. Front. Mar. Sci. 7 https://doi.org/10.3389/fmars.2020.00568.
Gordon, A.S., Donat, J.R., Kango, R.A., Dyer, B.J., Stuart, L.M., 2000. Dissolved copper-complexing ligands in cultures of marine bacteria and estuarine water. Mar. Chem. 70, 149–160. https://doi.org/10.1016/S0304-4203(00)00019-0.
Guillard, R.R.L., 1975. Culture of phytoplankton for feeding marine invertebrates. In: Culture of Marine Invertebrate Animals: Proceedings—1st Conference on Culture of Marine Invertebrate Animals Greenport. Springer, pp. 29–60.
Guillard, R.R.L., Ryther, J.H., 1962. Studies of marine planktonic diatoms: I. *Cyclotella nana* Hustedt, and *Detonula confervacea* (Cleve) gran. Can. J. Microbiol. 8, 229–239. https://doi.org/10.1139/m62-029.
Guo, J. (2012). Copper Requirements and Acquisition Mechanisms in Marine Phytoplankton. (Thesis). University of British Columbia. Retrieved from https://open.library.ubc.ca/collections/ubctheses/24/items/1.0053491.
Guo, J., Annett, A.L., Taylor, R.L., Lapi, S., Ruth, T.J., Maldonado, M.T., 2010. Copper-uptake kinetics of coastal and oceanic diatoms. J. Phycol. 46, 1218–1228. https://doi.org/10.1111/j.1529-8817.2010.00911.x.
Guo, J., Green, B.R., Maldonado, M.T., 2015. Sequence analysis and gene expression of potential components of copper transport and homeostasis in *Thalassiosira pseudonana*. Protist 166, 58–77. https://doi.org/10.1016/j.protis.2014.11.006.
Halliwell, B., Gutteridge, J.M.C., 1990. Role of free radicals and catalytic metal ions in human disease: an overview. Methods Enzymol. 186, 1–85. https://doi.org/10.1016/0076-6879(90)86093-B.
Harrison, G.I., Morel, F.M.M., 1986. Response of the marine diatom *Thalassiosira weissflogii* to iron stress. Limnol. Oceanogr. 31, 989–997. https://doi.org/10.4319/lo.1986.31.5.0989.
Herzi, F., Jean, N., Zhao, H., Mounier, S., Mabrouk, H.H., Hlaili, A.S., 2013. Copper and cadmium effects on growth and extracellular exudation of the marine toxic dinoflagellate *Alexandrium catenella*: 3D-fluorescence spectroscopy approach. Chemosphere 93, 1230–1239. https://doi.org/10.1016/j.chemosphere.2013.06.084.
Hudson, R.J.M., 1998. Which aqueous species control the rates of trace metal uptake by aquatic biota? Observations and predictions of non-equilibrium effects. Total Environ. 219, 95–115. https://doi.org/10.1016/S0048-9697(98)00230-7.
Hudson, R.J.M., Morel, F.M.M., 1990. Lron transport in marine phytoplankton: kinetics of cellular and medium coordination reactions. Limnol. Oceanogr. 35, 1002–1020. https://doi.org/10.4319/lo.1990.35.5.1002.
Hudson, R.J.M., Morel, F.M.M., 1993. Trace metal transport by marine microorganisms: implications of metal coordination kinetics. Deep-Sea Res. I 40, 129–150.
Hudson, R.J.M., Covault, D.T., Morel, F.M.M., 1992. Investigations of iron coordination and redox reactions in seawater using ^{59}Fe radiometry and ion-pair solvent extraction of amphiphilic iron complexes. Mar. Chem. 38, 209–235.
Janoš, P., Aupič, J., Ruthstein, S., Magistrato, A., 2022. The conformational plasticity of the selectivity filter methionines controls the in-cell Cu(I) uptake through the CTR1 transporter. QRB Discov. 3, e3 https://doi.org/10.1017/qrd.2022.2.
Johannessen, S.C., Macdonald, R.W., Burd, B., van Roodselaar, A., Bertold, S., 2015. Local environmental conditions determine the footprint of municipal effluent in coastal waters: a case study in the Strait of Georgia, British Columbia. Sci. Total Environ. 508, 228–239. https://doi.org/10.1016/j.scitotenv.2014.11.096.
Johnson, K.S., Gordon, R.M., Coale, K.H., 1997. What controls dissolved iron concentrations in the world ocean? Mar. Chem. 57, 137–161.
Juneau, P., El Berdey, A., Popovic, R., 2002. PAM fluorometry in the determination of the sensitivity of *Chlorella vulgaris*, *Selenastrum capricornutum*, and *Chlamydomonas reinhardtii* to copper. Arch. Environ. Contam. Toxicol. 42, 155–164. https://doi.org/10.1007/s00244-001-0027-0.
Kar, S., Sen, S., Maji, S., Saraf, D., Ruturaj, Paul, R., et al., 2022. Copper(II) import and reduction are dependent on His-Met clusters in the extracellular amino terminus of human copper transporter-1. J. Biol. Chem. 298, 101631 https://doi.org/10.1016/j.jbc.2022.101631.
Kazamia, E., Sutak, R., Paz-Yepes, J., Dorrell, R.G., Vieira, F.R.J., Mach, J., et al., 2018. Endocytosis-mediated siderophore uptake as a strategy for Fe acquisition in diatoms. Sci. Adv. 4 https://doi.org/10.1126/sciadv.aar4536.
Kim, B.-E., Nevitt, T., Thiele, D.J., 2008. Mechanisms for copper acquisition, distribution and regulation. Nat. Chem. Biol. 4, 176–185. https://doi.org/10.1038/nchembio.72.
Kim, J., Price, N.M., 2017. The influence of light on copper-limited growth of an oceanic diatom, *Thalassiosira oceanica* (Coscinodiscophyceae). J. Phycol. 53, 938–950. https://doi.org/10.1111/jpy.12563.
Knauer, K., Behra, R., Sigg, L., 1997. Effects of free Cu^{2+} and Zn^{2+} ions on growth and metal accumulation in freshwater algae. Environ. Toxicol. Chem. 16, 220–229. https://doi.org/10.1002/etc.5620160218.
Kong, L., 2022. Copper requirement and acquisition by marine microalgae. Microorganisms 10, 1853. https://doi.org/10.3390/microorganisms10091853.
Kong, L., Price, N.M., 2019. Functional CTR-type Cu (I) transporters in an oceanic diatom. Environ. Microbiol. 21, 98–110. https://doi.org/10.1111/1462-2920.14428.
Kong, L., Price, N.M., 2022a. Long-term adaptive response of an oceanic diatom to copper deficiency. Front. Mar. Sci. 9 https://doi.org/10.3389/fmars.2022.975184.
Kong, L., Price, N.M., 2022b. Transcriptomes of an oceanic diatom reveal the initial and final stages of acclimation to copper deficiency. Environ. Microbiol. 24, 951–966. https://doi.org/10.1111/1462-2920.15609.
Kroger, N., Sumper, M., 1998. Diatom cell wall proteins and the cell biology of silica biomineralization. Protist 149, 213–219. https://doi.org/10.1016/S1434-4610(98)70029-X.
Kustka, A.B., Allen, A.E., Morel, F.M.M., 2007. Sequence analysis and transcriptional regulation of iron acquisition genes in two marine diatoms. J. Phycol. 43, 715–729. https://doi.org/10.1111/j.1529-8817.2007.00359.x.
La Fontaine, S., Quinn, J.M., Nakamoto, S.S., Dudley Page, M., Göhre, V., Moseley, J.L., et al., 2002. Copper-dependent iron assimilation pathway in the model photosynthetic eukaryote *Chlamydomonas reinhardtii*. Eukaryot. Cell 1, 736–757. https://doi.org/10.1128/EC.1.5.736-757.2002.
Laglera, L.M., Battaglia, G., van den Berg, C.M.G., 2007. Determination of humic substances in natural waters by cathodic stripping voltammetry of their complexes with iron. Anal. Chim. Acta 599, 58–66. https://doi.org/10.1016/j.aca.2007.07.059.

Laglera-Baquer, L.M., González-Dávila, M., Santana-Casiano, J.M., 2001. Determination of metallic complexing capacities of the dissolved organic material in seawater. Sci. Mar. 65, 33–40. https://doi.org/10.3989/scimar.2001.65s133.

Larimer, F., Chain, P., Hauser, L., et al., 2004. Complete genome sequence of the metabolically versatile photosynthetic bacterium *Rhodopseudomonas palustris*. Nat. Biotechnol. 22, 55–61. https://doi.org/10.1038/nbt923.

Le Costaouëc, T., Unamunzaga, C., Mantecon, L., Helbert, W., 2017. New structural insights into the cell-wall polysaccharide of the diatom *Phaeodactylum tricornutum*. Algal Res. 26, 172–179. https://doi.org/10.1016/j.algal.2017.07.021.

Leal, P., Hurd, C., Sander, S., Armstrong, E., Roleda, M., 2016. Copper ecotoxicology of marine algae: a methodological appraisal. Chem. Ecol. 32 https://doi.org/10.1080/02757540.2016.1177520.

Long, M., Holland, A., Planquette, H., González Santana, D., Whitby, H., Soudant, P., et al., 2019. Effects of copper on the dinoflagellate *Alexandrium minutum* and its allelochemical potency. Aquat. Toxicol. 210, 251–261. https://doi.org/10.1016/j.aquatox.2019.03.006.

de Lurdes, M., Gonçalves, S., Sigg, L., Reutlinger, M., Stumm, W., 1987. Metal ion binding by biological surfaces: voltammetric assessment in the presence of bacteria. Sci. Total Environ. 60, 105–119. https://doi.org/10.1016/0048-9697(87)90411-6.

Maldonado, M.T., Allen, A.E., Chong, J.S., Lin, K., Leus, D., Karpenko, N., et al., 2006. Copper-dependent iron transport in coastal and oceanic diatoms. Limnol. Oceanogr. 51, 1729–1743. https://doi.org/10.4319/lo.2006.51.4.1729.

Martinez, R.E., Pokrovsky, O.S., Schott, J., Oelkers, E.H., 2008. Surface charge and zeta-potential of metabolically active and dead cyanobacteria. J. Colloid Interface Sci. 323, 317–325. https://doi.org/10.1016/j.jcis.2008.04.041.

McQuaid, J.B., Kustka, A.B., Oborník, M., Horák, A., McCrow, J.P., Karas, B.J., et al., 2018. Carbonate-sensitive phytotransferrin controls high-affinity iron uptake in diatoms. Nature 555, 534–537. https://doi.org/10.1038/nature25982.

Mendes, P., 1997. Biochemistry by numbers: simulation of biochemical pathways with Gepasi 3. Trends Biochem. Sci. 22 (9), 361–363. https://doi.org/10.1016/s0968-0004(97)01103-1.

Merchant, S.S., Allen, M.D., Kropat, J., Moseley, J.L., Long, J.C., Tottey, S., et al., 2006. Between a rock and a hard place: trace element nutrition in *Chlamydomonas*. Biochim. Biophys. Acta, Mol. Cell Res. 1763, 578–594. https://doi.org/10.1016/j.bbamcr.2006.04.007.

Moffett, J.W., Brand, L.E., 1996. Production of strong, extracellular Cu chelators by marine cyanobacteria in response to Cu stress. Limnol. Oceanogr. 41, 388–395. https://doi.org/10.4319/lo.1996.41.3.0388.

Moffett, J.W., Brand, L.E., Croot, P.L., Barbeau, K.A., 1997. Cu speciation and cyanobacterial distribution in harbors subject to anthropogenic Cu inputs. Limnol. Oceanogr. 42, 789–799. https://doi.org/10.4319/lo.1997.42.5.0789.

Monzyk, B., Crumbliss, A.L., 1982. Kinetics and mechanism of the stepwise dissociation of iron(III) from ferrioxamine B in aqueous acid. J. Am. Chem. Soc. 104, 4921–4929. https://doi.org/10.1021/ja00382a031.

Morrissey, J., Sutak, R., Paz-Yepes, J., Tanaka, A., Moustafa, A., Veluchamy, A., et al., 2015. A novel protein, ubiquitous in marine phytoplankton, concentrates iron at the cell surface and facilitates uptake. Curr. Biol. 25, 364–371. https://doi.org/10.1016/j.cub.2014.12.004.

Motschi, H., 1984. Correlation of EPR-parameters with thermodynamic stability constants for copper(II) complexes Cu(II)-EPR as a probe for the surface complexation at the water/oxide interface. Colloids Surf. A Physicochem. Eng. Asp. 9, 333–347. https://doi.org/10.1016/0166-6622(84)80176-6.

Nosenko, T., Lidie, K.L., Van Dolah, F.M., Lindquist, E., Cheng, J.F., Bhattacharya, D., 2006. Chimeric plastid proteome in the Florida "red tide" dinoflagellate *Karenia brevis*. Mol. Biol. Evol. 23, 2026–2038. https://doi.org/10.1093/molbev/msl074.

Omanović, D., Gamier, C., Pižeta, I., 2015. ProMCC: an all-in-one tool for trace metal complexation studies. Mar. Chem. 173, 25–39. https://doi.org/10.1016/j.marchem.2014.10.011.

Paasche, E., 1973. Silicon and the ecology of marine plankton diatoms. I. *Thalassiosira pseudonana* (*Cyclotella nana*) grown in a chemostat with silicate as limiting nutrient. Mar. Biol. 19, 117–126.

Paasche, E., 1977. Growth of three plankton diatom species in Oslofjord water in the absence of artificial chelators. J. Exp. Mar. Biol. Ecol. 29, 91–106.

Palenik, B., Kieber, D.J., Morel, F.M.M., 1989. Dissolved organic nitrogen use by phytoplankton: the role of cell-surface enzymes. Biol. Oceanogr. 6, 347–354.

Peers, G., Price, N.M., 2006. Copper-containing plastocyanin used for electron transport by an oceanic diatom. Nature 441, 341–344. https://doi.org/10.1038/nature04630.

Peers, G., Quesnel, S., Price, N.M., 2005. Copper requirements for iron acquisition and growth of coastal and oceanic diatoms. Limnol. Oceanogr. 50, 1149–1158.

Redfield, A.C., 1958. The biological control of chemical factors in the environment. Am. Sci. 46, 230A–221.

Ruacho, A., Richon, C., Whitby, H., Bundy, R.M., 2022. Sources, sinks, and cycling of dissolved copper binding ligands in the ocean. Commun. Earth Environ. 3, 263. https://doi.org/10.1038/s43247-022-00597-1.

Santiago-Díaz, P., Rivero, A., Rico, M., González González, A., González-Dávila, M., Santana-Casiano, M., 2023. Copper toxicity leads to accumulation of free amino acids and polyphenols in *Phaeodactylum tricornutum* diatoms. Environ. Sci. Pollut. Res. 30, 51261–51270. https://doi.org/10.1007/s11356-023-25939-0.

Sarathy, V., Allen, H.E., 2005. Copper complexation by dissolved organic matter from surface water and wastewater effluent. Ecotoxicol. Environ. Saf. 61, 337–344. https://doi.org/10.1016/j.ecoenv.2005.01.006.

Scarano, G., Morelli, E., 1999. Binding of Cu, Pb, Zn and Cd to the cell surface of the marine diatom *Phaeodactylum tricornutum*. Toxicol. Environ. Chem. 72, 93–104. https://doi.org/10.1080/02772249909358827.

Segovia, M., Lorenzo, M.R., Maldonado, M.T., Larsen, A., Berger, S.A., Tsagaraki, T.M., et al., 2017. Iron availability modulates the effects of future CO_2 levels within the marine planktonic food web. Mar. Ecol. Prog. Ser. 565, 17–33. https://doi.org/10.3354/meps12025.

Semeniuk, D.M., Cullen, J.T., Johnson, W.K., Gagnon, K., Ruth, T.J., Maldonado, M.T., 2009. Plankton copper requirements and uptake in the subarctic Northeast Pacific Ocean. Deep Sea Res. 1 Oceanogr. Res. Pap. 56, 1130–1142. https://doi.org/10.1016/j.dsr.2009.03.003.

Semeniuk, D.M., Bundy, R.M., Payne, C.D., Barbeau, K.A., Maldonado, M.T., 2015. Acquisition of organically complexed copper by marine phytoplankton and bacteria in the northeast subarctic Pacific Ocean. Mar. Chem. 173, 222–233. https://doi.org/10.1016/j.marchem.2015.01.005.

Sievers, F., Wilm, A., Dineen, D., Gibson, T.J., Karplus, K., Li, W., et al., 2011. Fast, scalable generation of high-quality protein multiple sequence alignments using Clustal Omega. Mol. Syst. Biol. 7 https://doi.org/10.1038/msb.2011.75.

Sunda, W.G., Huntsman, S.A., 1996. Antagonisms between cadmium and zinc toxicity and manganese limitation in a coastal diatom. Limnol. Oceanogr. 41, 373–387. https://doi.org/10.4319/lo.1996.41.3.0373.

Sunda, W.G., Tester, P.A., Huntsman, S.A., 1990. Toxicity of trace metals to *Acartia tonsa* in the Elizabeth River and southern Chesapeake Bay. Estuar. Coast. Shelf Sci. 30, 207–221.

Sutak, R., Camadro, J.-M., Lesuisse, E., 2020. Iron uptake mechanisms in marine phytoplankton. Front. Microbiol. 11 https://doi.org/10.3389/fmicb.2020.566691.

Turner, D.R., Whitfield, M., Dickson, A.G., 1981. The equilibrium speciation of dissolved components in freshwater and sea water at 25 °C and 1 atm pressure. Geochim. Cosmochim. Acta 45, 855–881. https://doi.org/10.1016/0016-7037(81)90115-0.

Twining, B.S., Baines, S.B., 2013. The trace metal composition of marine phytoplankton. Annu. Rev. Mar. Sci. 5, 191–215.

Van Den Berg, C.M.G., 1982. Determination of copper complexation with natural organic ligands in seawater by equilibration with MnO_2 II. Experimental procedures and application to surface seawater. Mar. Chem. 11, 323–342. https://doi.org/10.1016/0304-4203(82)90029-9.

Walsh, M.J., Goodnow, S.D., Vezeau, G.E., Richter, L.V., Ahner, B.A., 2015. Cysteine enhances bioavailability of copper to marine phytoplankton. Environ. Sci. Technol. 49, 12145–12152. https://doi.org/10.1021/acs.est.5b02112.

Whitby, H., van den Berg, C.M.G., 2015. Evidence for copper-binding humic substances in seawater. Mar. Chem. 173, 282–290. https://doi.org/10.1016/j.marchem.2014.09.011.

Winter, J., 2013. Using the Student's *t*-test with extremely small sample sizes. Pract. Assess. Res. Eval. 18 (10) https://doi.org/10.7275/e4r6-dj05.

Wood, A.M., Everroad, R.C., Wingard, L.M., 2005. Measuring growth rates in microalgal cultures. In: Andersen, R.A. (Ed.), Algal Culturing Techniques, Vol. 8. Elsevier, pp. 269–286.

Zhou, X., Wangersky, P.J., 1989. Production of copper-complexing organic ligands by the marine diatom *Phaeodactylum tricornutum* in a cage culture turbidostat. Mar. Chem. 26, 239–259. https://doi.org/10.1016/0304-4203(89)90006-6.